We are IntechOpen, the world's leading publisher of Open Access books
Built by scientists, for scientists

6,900
Open access books available

186,000
International authors and editors

200M
Downloads

Our authors are among the

154
Countries delivered to

TOP 1%
most cited scientists

12.2%
Contributors from top 500 universities

CLARIVATE ANALYTICS
BOOK CITATION INDEX
INDEXED

WEB OF SCIENCE™

Selection of our books indexed in the Book Citation Index
in Web of Science™ Core Collection (BKCI)

Interested in publishing with us?
Contact book.department@intechopen.com

Non Contact Measurement System with Electromagnets for Vibration Tests on Bladed Disks

Christian Maria Firrone and Teresa Berruti
Department of Mechanics, Polytechnic University of Turin (POLITO), Turin,
Italy

1. Introduction

In vibration testing one of the main concerns in the measurement of the forced response of vibrating structures is the coupling between the test article and the exciter. When the structural behaviour of the structure is pretty linear a hammer test allows getting a first idea of the resonant frequencies and mode shapes without perturbing the dynamic response. Unfortunately, real applications of structures whose behaviour is linear are rare. Usually, structures are made of components assembled together by means of joints whose behaviour may result highly nonlinear. Depending on the amount of excitation, joints can dramatically change the dynamic behaviour of the whole system and the modelling of this type of constraint is therefore crucial for a correct design. For this reason, tests are performed to characterize the contact parameters of joints focusing the attention in the material used in the application or extending the study by considering the whole components coupled by a particular geometry of joint. The characterization of joints in dynamics requires the knowledge of the amplitude of the exciting force which is usually set as a harmonic waveform whose frequency varies within a range of interest in the so called stepped-sine test which overcomes two limits of the hammer test. In fact, the stepped-sine test controls the force amplitude at each value of frequency in a given range by means of a feedback control which activates the measurement only when the target force is reached. Moreover a realistic value of force amplitude must be reached in order to explore the nonlinear behaviour of the structure. For this reason electromagnetic shakers are used by connecting the exciter to the test article by means of a stinger. Different strategies are used to detune the dynamics of the test article itself from the dynamics of the exciter , they are based on the design of the stinger or on the constraint of the shaker. Unfortunately, these strategies are not useful in particular applications where a small perturbation may introduce large changes in the dynamics of structures or in general it may interfere with the measurement of the physical phenomena. In turbomachinery, this is the case when the nonlinear friction damping of the blade root attachment to the disk is studied. The amount of damping introduced by the contact is very small, nonetheless it is still of the same order of magnitude of the structural damping of the blade and it can be increased by a proper design of the blade root geometry (dovetail, fir-tree, flat, crowned). A contact excitation of the blade like the one required by the electromagnetic shaker would perturb the measurement of the

friction damping, for this reason it is preferred to excite directly the base of the platform where the blade is attached. Another example is the study of the forced response of rotors excited by a multiple source of excitation, which is the application of the study presented in this chapter. Two main features of the bladed disk design concerning the dynamic response are veryimportant. 1) The rotor is subjected to an excitation pattern where each blade is loaded with a series of pulses within a complete disk rotation. The number and the intensity of pulses depend on the architecture of the engine preceding the rotor (number of combustion chambers, stages, stator vanes) and the wide spectral content is usually characterized by several harmonic components whose excitation frequencies are mainly a multiple of the rotor angular speed. The harmonic index which defines the multiplicity is called *Engine Order* (*EO*). 2) A rotating disk is nominally characterized by cyclic symmetry properties (Thomas, 1979) where one fundamental sector constituted by the blade and its associated disk sector is repeated for a number of times around the rotation axis. The periodical repetition of geometric and material features (*tuned* configuration) generates a particular dynamic behaviour of the disk where natural frequencies, and corresponding modes, can be grouped into families featuring the same deformed shape of the vibrating blades and disk (Castanier & Pierre, 2006).

The main objective at design stage is to avoid any matching of the rotor natural frequencies with the excitation frequency of each harmonic component of the load spectrum which shortens the life of the component due to HCF failure of blades. Unfortunately, bladed disk dynamics may show unexpected response due to small differences between sectors nominally identical which determine a *mistuned* configuration of the system (Castanier & Pierre, 2006, Kenyon & Griffin, 2003). In worst cases, a distorted and localized forced response occurs in particular for high modal density regions where one or more blades vibration amplitude is higher than the tuned response amplitude. Causes of mistuning are multiple: irregularities associated to the material properties constituting the blades, asymmetry generated during assembly or during service due to wear assessment, different contact condition at the blade root joints, snubbers, shrouds in case of non-integral bladed disks, Foreign Object Damage (FOD) or modifications introduced during maintenance and repair processes. Another source of mistuning comes from the so-called underplatform dampers (UPDs) which are metal parts located within cavities between contiguous blades. UPDs' aim is to limit the vibration amplitude of blades in case of excitation at resonance by means of friction damping at the contact surfaces. Mistuning is introduced at the contacts which couple directly the blades subjected to wear and change of the contact position during service. Interesting studies were carried out where UPDs are seen not only as a further source of mistuning to take into account but also as a mean to mitigate negative effects of inherent mistuning (Pierre et al., 2002, Petrov et al., 2010) even by distributing a number of UPDs smaller than the number of the blades (Avalos & Mignolet, 2008) or by systematically using UPDs having different mass (Gotting et al., 2004).

Fimite Element Modelling, mistuning identification and numerical results obtained by taking into account mistuning in the design must be validated with tests on dummy or real disks. Test campaigns are performed on test rigs which can be classified in two groups having a basic dual property: the first group has rotating disks with fixed excitation source, on the contrary the second group supports a static rotor excited by a travelling excitation. Both test rigs have advantages and limitations which must be addressed with respect to the objective of the test campaign.

Rigs with rotating test articles are generally more complex than static rigs, first of all due to the design of the disk containment which must fulfil safety requirements in case of blade release (usually they are built in a pit or within a protective bunker). Moreover, different levels of complexity are found in the comprehension of the mistuning phenomenon if tests are performed on real engines and cold flow rigs since fluid-structure interaction must be considered. In detail, correlations between mistuning and aero-coupling, damping and elastic effects of gas flow which decreases the magnification factor of the mistuned response (Beirov et al., 2008) and the influence of mistuning on flutter instabilities onset can be studied. On the contrary, fluid-dynamics effects can be avoided in vacuum chamber (spin test rig). For both types of rotating rigs, however, gyroscopic and centrifugal force effects (e.g., blades untwisting, dependence of UPDs contact pressure on disk velocity) should be taken into account. The excitation provided by the gas flow must be substituted in vacuum rigs with an alternative source. Broad applications of non-contact excitation provided by magnetic fields are found in literature by means of permanent magnets or electromagnets whose attractive force is exerted on ferritic bladed disks. Permanent magnets are compact, not expensive exciters which can be easily bought at different material grade of magnetization working in some cases at a temperature up to 200°C. One blade is excited by the magnets which are equally spaced around the circumferential coordinate and is loaded during one disk rotation with a number of pulses equal to the number of magnets. The excitation frequency is therefore strictly proportional to the rotation frequency by the number of magnets which determines the engine order of the force pattern. Electromagnets allows to release the excitation frequency from the rotation speed by using an AC feeding (Prchlik et al., 2009) in spite of a more complexity of the excitation system: more room is required to place the EMs, heat must be dissipated (which can be a critical issue in vacuum), an amplifier system and a signal generator must be provided. Hybrid solution can be also found in literature as in (Rice et al., 2007) where magnetic excitation is used as an extra source of excitation in engine tests with gas flow in order to explore flutter onset at different engine orders for the same rotation speed i.e., for the same aerodynamic load, air mass flow and centrifugal effects. Moreover in (Szwedowicz et al., 2007) a really cheap exciter is constituted by an air jet simply generated by the pressure drop between room condition and the vacuum chamber. In this case only one exciter can be provided since it is not possible to control a given time delay between more pipes which are necessary if an engine order type excitation is required. On the contrary, a narrow, single pulse virtually contains all the engine order indices which can be calculated by Fourier series decomposition of the force profile along the spatial domain of the disk circumferential coordinate. A contacting excitation system is used in (Szwedowicz et al., 2006, Gilbert et al., 2010) by means of piezoelectric actuators applied to the root of the blades. Piezo-actuators need electric feeding supplied by an end-shaft slip-ring connected to the shaft. Since they are contacting devices, on one hand this technique may cause non-intentional mistuning which should be taken into account. On the other hand, a precise force control is achievable through the calibration of the piezo-devices. However, the dynamic perturbation induced by the exciters can be limited if they are glued to the disk (disk mistuning) which usually does not generate critical mistuning phenomena as perturbed blades do (blade mistuning).

The determination of the magnification factor requires the measurement of each blade response typically obtained by means of strain gauges which are again contacting devices

which can cause a non-intentional blade mistuning (Beirov et al., 2009). Tip timing techniques (Heath & Imregun, 1998, Heinz et al., 2010) proximity probes and rotating laser Doppler vibrometer (LDV) purposely designed (Sever, 2004) or already available in commerce are valid equipments which do not interfere with the original bladed disk dynamics. The first two techniques measure the disk response with respect to a stationary reference system while the third technique allows measuring the disk response on a reference system rotating with the disk. Therefore, attention must be paid to correlate input and output data of the rig with simulation results since the transformation of the coordinate system from static to rotating and vice versa is required. A not negligible aspect involving LDV measurement is the necessity of visual access to the rotating bladed disk which may be in conflict with safety requirements.

The second group of test rigs carries a static rotor and a rotating excitation. The travelling wave is in this case generated by contacting (piezo-actuators (Kruse & Pierre, part II, 1997), shakers (Strehlau & Kuhhorn, 2010)) or non-contacting systems (electromagnets with AC feeding (Kruse & Pierre, part I, 1997), speakers (Judge et al., 2003, Jones & Cross, 2010)). Whatever the case, a control system must be purposely developed in order to activate the exciters with a given phase shift in time to mimic the engine order force pattern. Since the bladed disk does not rotate, the dynamic response is directly measured on the reference system fixed to the rotor by using the same devices already described. In particular, the rotating LDV is substituted with a scanning LDV which measures, in its basic configuration, a set of points previously defined on the plane including the rotor (Strehlau & Kuhhorn, 2010, Berruti et al., 2010). Compared to the case of rotating rotors in this case aerodynamic coupling effects are avoided as well as complications given by data transmission. Such test rigs allow to easily collect measurements of the dynamics of dummy or real bladed disks directly related to mistuning and are therefore suitable for validating mistuning identification methods and reduction techniques with precision.

When non-linear phenomena are present as friction damping occurring at joints, the control of the force input is of primary importance since the forced response is strongly influenced by the amount of the local displacements of the structure at the contact surfaces. The force pattern can be measured during tests or estimated by means of a calibration process. Forces generated by air jets, for instance, can be measured with manometer probe measuring the pressure field before testing (Chang & Wickert, 2002) or with probes embedded in the surface of the blades (Petrov, 2010) or estimated as in (Szwedowicz et al., 2007) by calculating analytically the peak force applied to the blade as the product of the velocity at the end of the pipe and the mass flow hitting the blade. In this case the calculation relies on some simplifications about the area of the impacting gas and the distribution of the pressure on the blade airfoil. A similar approach can be used for oil jets whose higher density is suitable to excite very large blades. Much lower force amplitudes can be reached by speakers which can be calibrated by recording the spectra of a white noise by means of a microphone (Judge et al., 2003, Jones & Cross, 2010). The dynamics of the speaker can be recorded and used as a calibration curve in order to guarantee the same intensity at each frequency, while the value can be estimated by measuring the pressure on the microphone multiplied by the area of the speaker. Attention must be paid to the air gap between each blade and speaker since a small difference can cause an unacceptable error on the time delay between the harmonic force profiles which actually load the blades.

Force measurement using the magnetic field as a source of excitation can be performed by placing a force transducer below the magnet. In the case of permanent magnets, since it is usually a single piece, compact device, it can be considered as an additional mass which must be taken into account in order to verify if the frequency upper limit of the force transducer drops to values within the tested bandwidth. In the same way, force transducers can be used with electromagnets. Unfortunately, electromagnets are more complex devices than the permanent magnets, since components like conducting wires, packed plates, and insulating materials are assembled together and may generate a non-linear dynamic behaviour of the exciter itself. Similar to piezo-actuators (Kruse & Pierre, part II, 1997), they must be supported by an adequate power amplifier system in order to generate the required force amplitude in particular for high frequencies if non-linear dynamics characterization induced by slipping phenomena is addressed.

In this chapter, the design, manufacture and calibration of a travelling wave excitation system for bladed disks is described and tested. The typical application of the system is the Frequency Response Function (FRF) measurement by means of the stepped-sine technique for the characterization of the complex phenomenon of mistuning and non-linear dynamic response in presence of friction contacts such as blade root joints, shrouds or underplatform dampers. The measurements provide accurate results to be compared with numerical prediction.

The essential requirements of a travelling wave excitation system for such kind of tests in presence of mistuning are:

- the absence of contact between blade and exciter
- the same excitation force amplitude on each blade modulated with a given time lag which is determined by the engine order index.

If the test setup involves the characterization of nonlinearities due to friction the requisites listed above are not enough, since the excitation system should be able to provide also:

- a high excitation force amplitude in order to produce slipping between the friction contacts,
- an accurate measurement of the force amplitude of the rotating force pattern.

The excitation produced by an array of electromagnets (EMs) is non-contact and is then suitable for this kind of measurements. Moreover, any travelling wave force can be generated on the disk by changing the phase delay of the waveform of each current signal flowing on the EMs. The system hardware and software are purposely designed to satisfy all the requirements listed above. The system set up requires an accurate calibration process to generate the travelling force applied to the structure by each EM. The calibration consists of two steps: the first step is based on an instrumented EM which measures the force exerted on the structure, the second step is a tuning process in order to regulate all the other EMs for the generation of the same force amplitude on each blade.

In the first part of the chapter the hardware and software of the excitation system setup are described, together with a summary of the theoretical background that is necessary for the EM design. In the second part the system set up and calibration is presented by focusing on the proposed tuning method that allows the calibration of the EMs on site i.e., under the disk in their final position. In the last part of the chapter an example of application on a dummy bladed disk is presented.

2. The excitation system

The excitation system sketched in Figure 1a) is based on an electromagnetic unit, that is the electromagnet + the aluminium support (EM) repeated cyclically in order to excite a cyclic structure like a blade array where one EM is placed under each blade (Berruti et al, 2010, 2011). Each EM is mounted with a certain gap with respect to the blade so that the blade is not in contact with the exciter. The force is generated by the magnetic induction flowing through the EM, the air gap and the ferromagnetic material of the blade. The EMs are mounted on an aluminium circular plate (Figure 1-b). The aluminium is chosen in order to not interfere with the magnetic flux flowing in the EMs. Each EM is fed with a voltage with a given amplitude and phase. The signal generator system National Instruments cRIO 9074 is connected to the audio amplifiers Crown CDi 2000 (2 channels each, 800 W power supply for each channel). Each EM is connected to one channel. A LabVIEW software is purposely developed in order to generate a number of voltage harmonic signals equal to the number of EMs. The voltage signals are amplified in order to feed the EMs with a given amplitude and phase. The resulting excitation system has the following features:

- by feeding each EM with a voltage with a different phase from the neighboring it is possible to reproduce an engine order (EO) type excitation typical of the excitation of turbine disks in the engine;
- by controlling the force amplitude it is possible to keep it constant during the step-sine test;
- by tuning the EMs with respect to a reference one it is possible to reach the same excitation force amplitude on each EM.


(a)   (b)
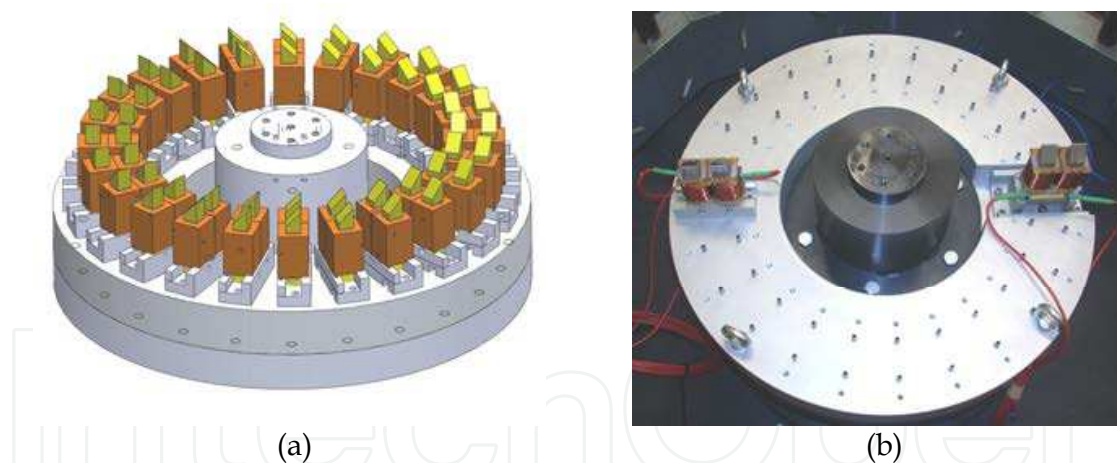
Fig. 1. a) The cyclical excitation system; b) The aluminium circular plate with two EMs.

2.1 The electromagnet unit design

The electromagnet design strictly depends on the type of application. The general design criteria are hereinafter addressed. The electromagnet is designed in order to satisfy two essential criteria related to i) the geometry of the cyclic structure (bladed disk) excited by the EM and ii) the maximum force and maximum frequency of the planned travelling wave excitation, in detail:

- the EM size must be limited according to the room between two adjacent blades of the disk under test. As an example, the bladed disk shown later in the application allows a

maximum square cross area for a commercial EM core S=16x16mm². The U-shaped core outer dimensions are therefore automatically determined: 64X48x16 mm.
- the EM must produce a force amplitude up to 10N in a mechanical frequency range from 100Hz to 600Hz given an average air gap l_{air}=2mm minimum. The last parameter is set in order to consider the variation of the gap during vibration negligible. For this reason l_{air} will be considered constant during the design process.

Figure 2 shows the designed EM unit which must face the blade with a gap that can be adjusted according to the application. Each electromagnet is made of two coils (1) of wire wrapped around a U-shaped core of ferromagnetic packed plates. Two prismatic ferromagnetic extensions (2) are glued at the two ends of the U shaped core in order to face the blade at the stagger angle α. This solution was preferred instead of producing a single piece EM core in order to change the prism in case of bladed disks with different stagger angles. The prismatic extensions are made up of SMC, i.e. a sintered ferromagnetic material which strongly limits the eddy currents.
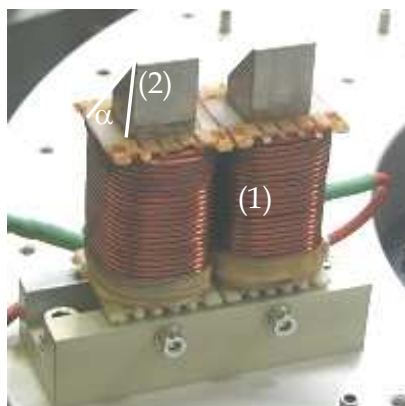
Fig. 2. Detail of the EM unit.

2.2 The theoretical model of the magnetic force

The attractive force on the blade can be estimated by means of a simple model of the magnetic circuit of the electromagnet facing the blade. Electromagnet and the equivalent magnetic circuit are sketched in Figure 3 a) and b) respectively. The two coils are modelled as two generators of magnetomotive force Ni, where N is the number of turns for each coil and i is the current. The part of the circuit corresponding to the air and the part of the circuit corresponding to the ferromagnetic materials are characterized by the values of the reluctance $\Re$:

$$\Re = \frac{l}{\mu S} \tag{1}$$

where l and S are respectively the length and the cross area of the part of the circuit characterized by $\Re$, μ is the magnetic permeability. $\Re_{steel}$ is the magnetic reluctance of the steel core and of the steel blade facing the electromagnet while $\Re_{air}$ is the magnetic reluctance of the air gap. $\Re_{steel}$ is much less than $\Re_{air}$ since $\mu_{steel} >> \mu_{air}$. The circuit can then be simplified with the circuit of Figure 3 c) where $\Re_{steel}$ is neglected.
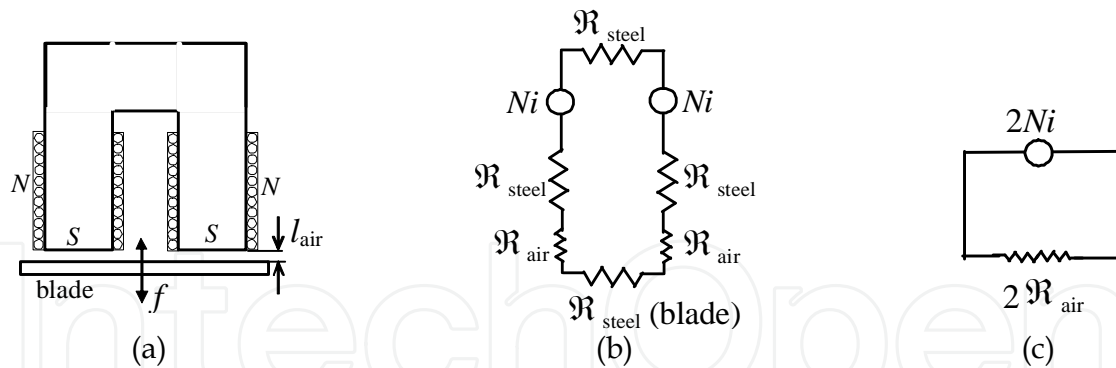
Fig. 3. a) Sketch of the electromagnet facing the steel blade; b) Equivalent magnetic circuit; c) Simplified equivalent magnetic circuit.

The following relationships can be written for the circuit of Figure 3 c):

$$2Ni = 2\mathfrak{R}_{\text{air}}\Phi \rightarrow 2Ni = 2\frac{l_{\text{air}}}{\mu_{\text{air}}S'}\Phi$$

$$2Ni = 2\frac{l_{\text{air}}}{\mu_{\text{air}}}B \rightarrow B = \frac{Ni \cdot \mu_{\text{air}}}{l_{\text{air}}}$$

$$(2)$$

where Φ is the magnetic flux, l_{air} is the air gap, S' is the area of each coil of the EM facing the blade ($S'=S/\sin(\alpha)$), B is the magnetic induction. The attractive force f exerted from the EM on the blade is the sum of two forces f_{coil} exerted by the two branches and is related to the magnetic induction B by the following relationship (principle of conservation of energy):

$$f = 2f_{\text{coil}} = 2\left(\frac{B^2 \cdot S'}{2 \cdot \mu_{\text{air}}}\right)$$

$$(3)$$

Substituting Eq.(2) in Eq.(3), the following relationship between the force and the current holds:

$$f = \frac{(Ni)^2 \cdot \mu_{\text{air}} \cdot S'}{l_{\text{air}}^2}$$

$$(4)$$

When the electromagnet is fed by an alternating current $i(t) = I\sin(\omega t + \varphi)$, with ω electrical angular frequency $\omega = 2\pi f_{el}$ (being f_{el} the electrical frequency in Hz) and φ a given phase shift, the force in Eq.(4) becomes:

$$f = \frac{N^2 \cdot \mu_{\text{air}} \cdot S'}{l_{\text{air}}^2}I^2 sen^2(\omega t + \varphi) = \frac{N^2 \cdot \mu_{\text{air}} \cdot S'}{l_{\text{air}}^2}\frac{I^2}{2}\left(1 - \cos(2\omega t + 2\varphi)\right) = f_s + f_a$$

$$(5)$$

where f_s and f_a are the static and the alternate component of the attractive force. The alternate component of the attractive force becomes:

$$f_a = \frac{(N \cdot I)^2 \cdot \mu_{\text{air}} \cdot S'}{2l_{\text{air}}^2}\cos(2\omega t + 2\varphi) =$$

$$= F_A\cos(2f_{el} \cdot 2\pi t + 2\varphi) = F_A\cos(f_m \cdot 2\pi t + 2\varphi)$$

$$(6)$$

The force f_a is the force that excites dynamically the blade at the mechanical frequency $f_m = 2 f_{el}$. The blades are then excited with a "mechanical" frequency f_m that is two times the "electrical" frequency f_{el}.

The force amplitude F_A is determined by the product NI. The current amplitude should be limited to a maximum value of 10A in order to avoid risk for the insulation due to the generation of heat.

In the next paragraph the relationship between the exciting force amplitude F_A and the value of the voltage amplitude V generated by the amplifier is given, since it is of more practical use to know the value of voltage that must be generated by the amplifier in order to excite each blade at a desired force.

2.3 The electrical circuit model

In order to characterize the electrical circuit of the EM the amplitude value of the AC current I is measured for different values of amplitude and frequency of the AC applied voltage V. Figure 4 shows the value of the measured current amplitude I versus the input voltage amplitude V for different frequency values. Note that the trends are linear and for a given voltage value the current (and therefore the amplitude of the force F_A, Eq.(6)) flowing in the EM decreases as the frequency increases. The admittance quantity $Y = I/V$ is diagrammed in Figure 5 (experimental values are presented with black dots). Y is a useful quantity which characterizes the EM in order to know what is the current (and then the actual force) that can be expected given a value of voltage V (representing the generated signal) at a given frequency. This information is of primary importance if controlled force, step-sine tests must be performed. In this case in fact, the voltage must vary during the frequency sweep in order to guarantee the same output current amplitude and therefore the same force amplitude.

Assuming a simple RL model of the electrical circuit the value Y can be calculated as:

$$Y = \frac{1}{\sqrt{R^2 + \omega^2 L^2}} \tag{7}$$

where R is the resistance, L the inductance and ω the angular frequency. The R value is measured at the winding ends ($R=0.3\ \Omega$). The L value (5.5 mH, standard deviation 0.7 mH) is estimated from Eq.(7) as a mean value of all the inductances calculated from each measured Y values. The comparison of the calculated trend of Y (solid line) with the "measured" Y in Figure 5 shows a good agreement. The simple RL model can be therefore used to calculate the value of Y also outside the measured points. Substituting Y which includes the information about the electrical frequency, $I=Y(\omega)V$, in Eq.(6):

$$f_a = \frac{(NV)^2 \cdot \mu_{\text{air}} \cdot S'}{2 \cdot (R^2 + \omega^2 L^2) l_{\text{air}}^2} \cos(2\omega t + 2\varphi) =$$
$$= F_A \cos(2\omega t + 2\varphi) \tag{8}$$
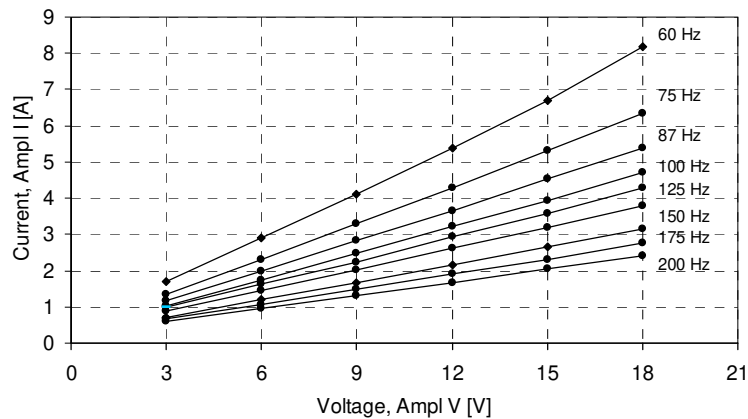
Fig. 4. Measured output current amplitude vs. input voltage amplitude for different input voltage frequency.
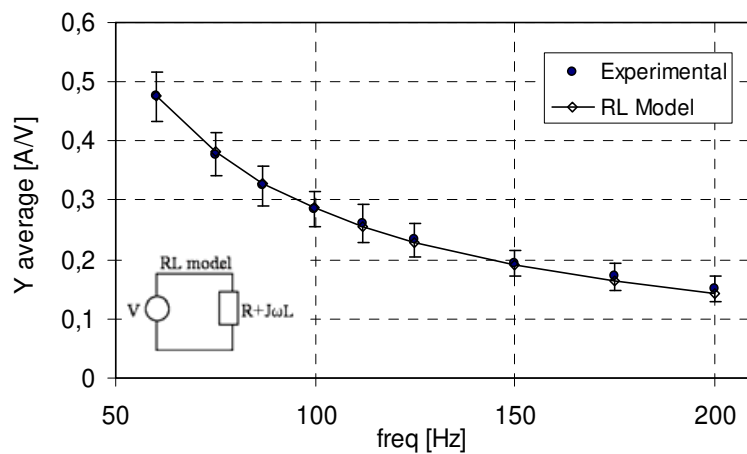

Fig. 5. Comparison of admittance values Y derived from experiments and from *RL* model.

Equation (8) shows the relationship between the voltage amplitude *V*, the force amplitude F_A and the input electrical frequency (ω):

$$V^2 = \frac{2 \cdot F_a \cdot \left(R^2 + \omega^2 L^2 \right) \cdot l_{\text{air}}^2}{\mu_{\text{air}} N^2 \cdot S'} \tag{9}$$

Since $R^2 << \omega^2 L^2$ (R=0.3 Ω, L = 5.5 mH, Berruti et al., 2010, 2011) the term R^2 can be neglected. Considering also that $\omega = 2\pi f_{el}$, Eq. (9) can be rewritten in the two forms:

$$V = \left(\sqrt{\frac{4 \cdot \pi^2 \cdot F_A \cdot L^2 \cdot l_{\text{air}}^2}{\mu_{\text{air}} N^2 \cdot S'}} \right) \cdot f_{el}$$

$$V = \left(\sqrt{\frac{4 \cdot \pi^2 \cdot f_{el}^2 \cdot L^2 \cdot l_{\text{air}}^2}{\mu_{\text{air}} N^2 \cdot S'}} \right) \cdot \sqrt{F_A} \tag{10}$$

The two relationships in Eq. (10) put in evidence that for a given value of the excitation force amplitude F_A, the corresponding value of the voltage *V* feeding the EM changes

proportionally with f_{el}. In the same way, for a given frequency value f_{el}, the voltage amplitude value V changes proportionally with $\sqrt{F_A}$. These two linear trends of Equation (10) (V vs. f_{el} and V vs. $\sqrt{F_A}$) will be confirmed by the experimental tests as shown in the following sections. The formulas presented in this paragraph are useful to understand the dependence of the output parameter of the exciter (force amplitude F_A varying harmonically with a given frequency f_m) from the input parameter (the voltage amplitude V varying harmonically with a given frequency f_{el}) and to decide the dimension of the EM according to the maximum force that is generated, but are not sufficient to determine the exact numerical values since some parameters like the inductance L, the air gap l_{air} or the active cross section in front of the air gap S' are not known with precision. For this reason a direct calibration of the EMs is required as described in the following paragraph.

2.4 Calibration of the EMs

The EMs used in the multiple excitation system are nominally identical, however, in order to check the EMs manufacture quality, each EM unit is calibrated on a calibration bench shown in Figure 6 a). A force transducer (1), carrying a ferromagnetic anchor (2), is connected to an inertial mass (3). The anchor has the same local shape and size of the disk blade that is tested. The part of the inertial mass close to the anchor is made of aluminum (4) in order to not interfere with the magnetic flux. The EM faces the anchor with a given gap (2 mm). A control software developed in Labview is here used to adjust the harmonic input voltage of the EM amplifier in order to obtain the desired force amplitude (with a tolerance of ±1%) measured by the force transducer connected to the anchor.
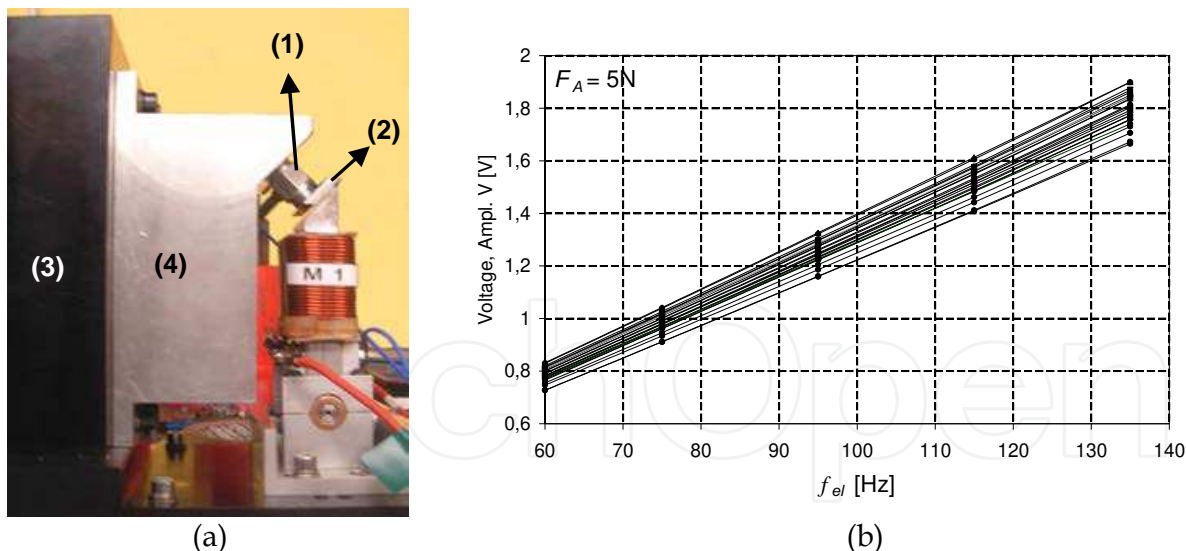

Fig. 6. a) The EM on the calibration bench; b) The 24 EMs calibration curves.

In Figure 6 b) the calibration curves defined as the input voltage amplitude (V) vs. the input electrical frequency (f_{el}) are shown for the 24 electromagnets that are used later in the application by keeping the force amplitude F_A = 5N constant on the anchor. The repeatability error on the measured voltage values obtained by repositioning the same EM on the rig is 2% maximum. Despite the good calibration repeatability and the nominal equal shape, the calibration curves of the 24 EMs are different from each other. The highest

voltage difference for the same electrical frequency is 13% with respect to the mean value . The difference of the calibration curves is associated to the EM manufacture process. The linear trend of the calibration curves in Figure 6 b) confirms the validity of the relationship of Eq.(10) where the amplitude voltage V is proportional to the electrical frequency f_{el} for a given force amplitude F_A.

2.5 The control of the excitation force amplitude

The control of the excitation force amplitude is obtained by means of a device, called Force Measuring ElectroMagnet (FMEM) which allows the measurement of the force exerted by one EM (Firrone & Berruti, 2011). The device is shown in Figure 7 a). The FMEM includes an EM nominally equal to the other EMs which is mounted on a particular support carrying a piezoelectric force transducer (1). The transducer measures the horizontal component (F_M) of the force (F_A) produced by the EM and applied to the blade. The reaction of the vertical component of F_A as well as the mass of the EM is supported by the vertical leaf spring at the base of the FMEM. By knowing the relationship occurring between F_A and F_M at different frequencies, it is possible to control the force F_A applied to the blade by controlling the force F_M measured by the force transducer.
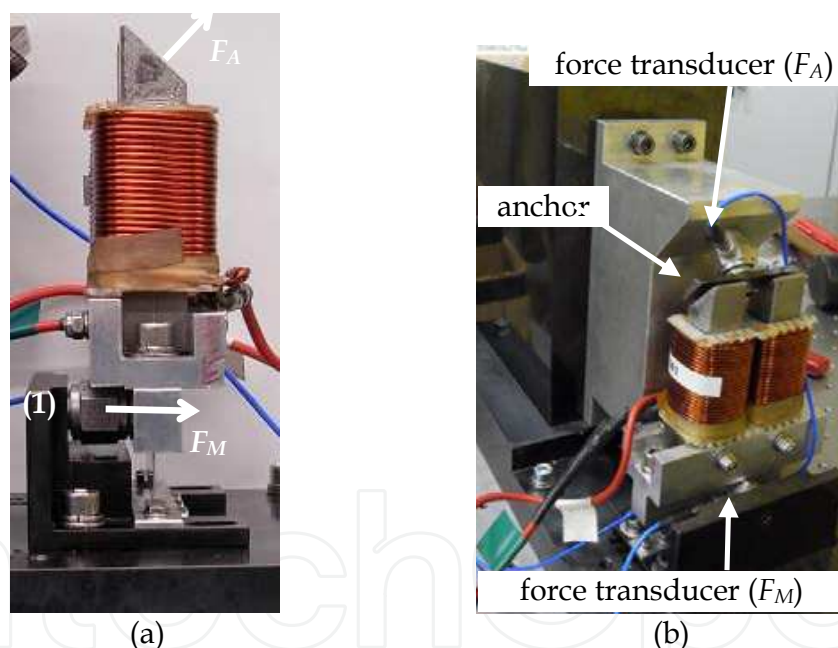
Fig. 7. a) The force measuring electromagnet (FMEM); b) the FMEM on the calibration bench.

The FMEM needs a special calibration process in order to establish the relationship between the force F_A and the force F_M measured by the force transducer (1) at different frequencies. The FMEM is therefore calibrated on the same calibration bench used for the other EMs as shown in the picture of Figure 7 b).

The FMEM faces the anchor with a given gap (2 mm). Once the harmonic force amplitude F_A is controlled by the software to a given value, the force amplitude F_M is measured by the FMEM transducer and recorded. The plot F_M/F_A vs. f_{el} is the calibration curve shown in Figure 8.
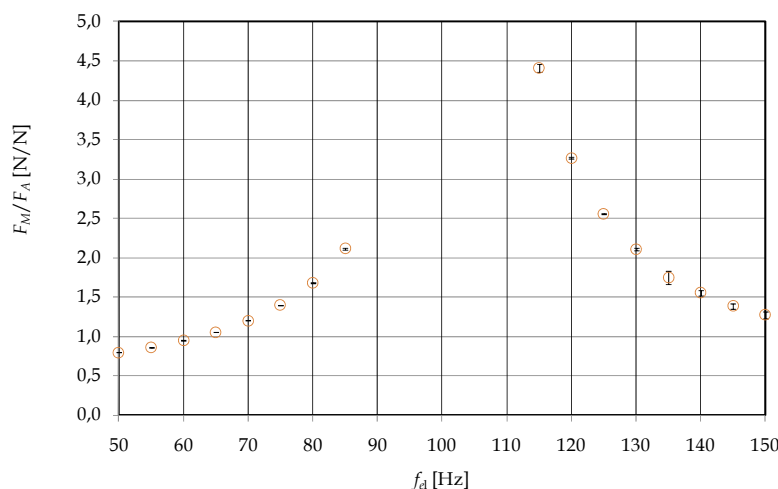
Fig. 8. The FMEM calibration curve.

The curve of Figure 8 shows that the FMEM has a natural frequency within the range of interest. A hammer test confirmed the presence of a natural frequency of the FMEM at 206 Hz (which corresponds to f_{el} = 103 Hz). In order to avoid the resonance condition of the FMEM that can lead to a poor measurement repeatability, the FMEM will be employed only in the ranges of frequency outside the resonance (f_{el} = 50→75 Hz and f_{el} = 140→150 Hz).

2.5.1 Reliability of the FMEM on the calibration bench

In order to estimate the reliability of the force amplitude value imposed and controlled by means of the FMEM, different calibration tests are performed on the calibration bench of Figure 7 b). The tests are listed below.

1. Check of the force control. Calibration curves are measured for different nominal values of the force on the anchor (F_{Anom} =1, 2, 3 , 4, 5, 6 N) with the same air gap of 2 mm. As a result, for each F_{Anom} a calibration curve like that of Figure 8 is obtained. An "inverse calibration" is then performed on the same bench in order to simulate the same control force procedure that will be used on site under the bladed disk. In this case the FMEM transducer that measures F_M is controlled by the software. The set-point controlled by the software at different frequencies is $F_M = (F_M/F_A) \cdot F_{A,nom}$ where $F_{A,nom}$ is the nominal force value and (F_M/F_A) is the calibration curve. When the FMEM transducer reaches the target value F_M, the actual force $F_{A,act}$ exerted on the anchor is measured. The difference between the measured value $F_{A,act}$ and the nominal value $F_{A,nom}$ proved to be always within 1% of $F_{A,nom}$ for all the tested frequencies confirming the quality of the force control procedure.

2. Check of the FMEM repeatability. $F_{A,nom}$ is set to 5 N, and the air gap to 2 mm. Different calibration curves F_M/F_A are obtained after repositioning the FMEM on the calibration bench. The calibration curve F_M/F_A plotted in Figure 8 is the average result $(F_M/F_A)_{AVG}$. The "inverse calibration" is then performed by controlling the force value F_M measured by the transducer on the FMEM support. The set-point controlled by the software at

different frequencies is calculated as $F_M=(F_M/F_A)_{AVG}·F_{A,nom}$. When the FMEM transducer reaches the target value F_M, the actual force $F_{A,act}$ exerted on the anchor is measured. The error of $F_{A,act}$ with respect to the nominal force value of 5N is 3% in the worst case.

It can then be concluded that after this calibration procedure it is possible to obtain the desired value of force amplitude F_A on the anchor with a precision inside 3% by controlling the force F_M on the FMEM support.

3. The test rig

The excitation system is designed to study the complex dynamics of bladed disks for turbomachinery applications. In detail, the aim is to collect a database of measurements on real or dummy bladed disks in order to highlight the effect of mistuning and friction damping. The experimental results will be compared with results from numerical simulation tools. The multiple excitation system described above is set up on the test rig *Octopus* designed to test bladed disks carrying underplatform dampers (UPDs) between the blade platforms (Berruti, 2010). The test rig shown in Figure 9 a) can be divided into two parts, i.e., the central support carrying the real or dummy disk and an outer ring supporting the arm structures used to couple the bladed disk with the UPDs. The required number of arms depends on the number of blades of the specific disk. In this case the test rig is prepared to test a dummy integral bladed disk (*blisk*) with 24 blades, therefore a number of $N_b=24$ arms must be provided. Nevertheless, the outer ring can be used in part or can be extended depending on the specific disk and its number of blades. Figure 9 a) shows the test rig with the dummy blisk (1) already mounted on it.

(a)   (b)
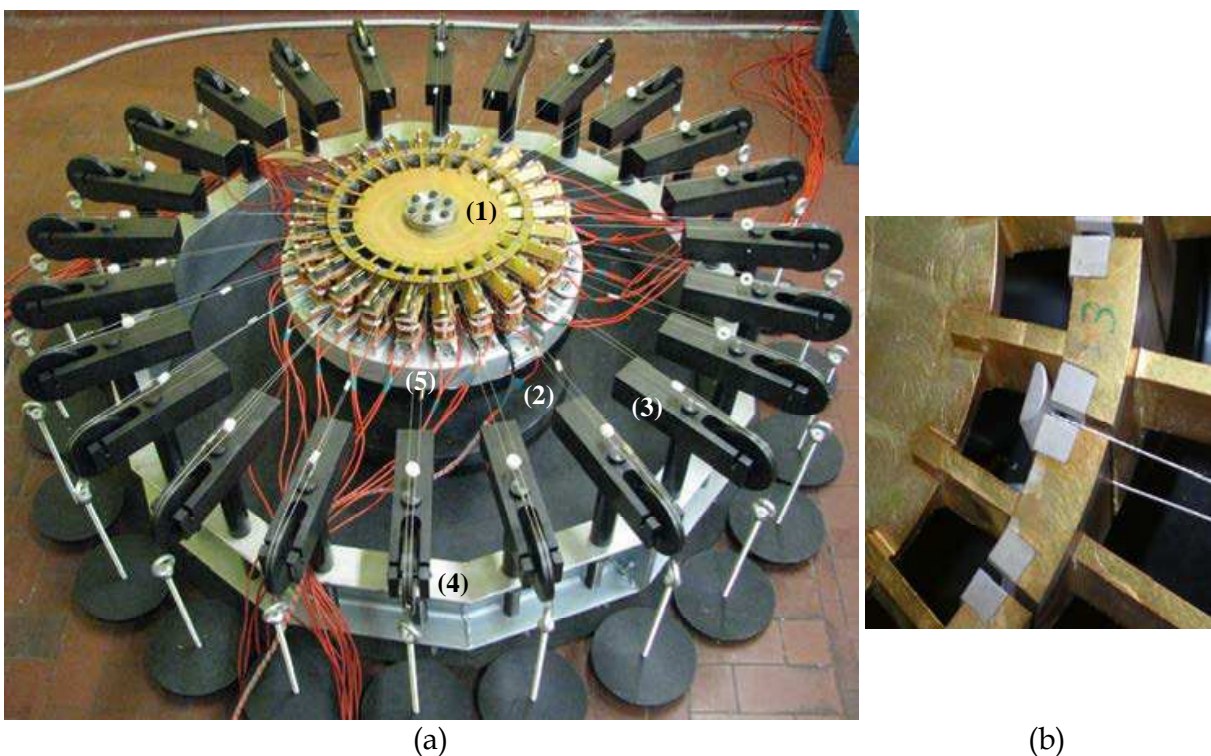
Fig. 9. a) The test rig Octopus; b) detail of the UPD.

The blisk is constrained on the central fixture (2), which is basically a big inertial mass (about 400kg) with two coaxial cylinders mounted on a circular plate laid on a rubber sheet. The arm structures (3) support one pulley each and are equally spaced around the fixture. Two wires attached to each UPD (Figure 9 b)) pass over the arm supporting the pulley and are connected to a loading plate which carries dead weights simulating the centrifugal force on the UPD. The pulley has low friction ball bearing and is mounted on a pin tightened on the circular outer ring (4) (about 1.5m diameter) centered with respect to the disk fixture. Each arm carrying the pulley can rotate around the pin in order to align with precision the wires along the radial direction of the centrifugal force acting on the UPDs. The outer ring is fixed to the floor and is not directly connected to the central fixture in order to minimize the transmission of vibrations from the fixture to the ring. The dummy blisk is centered on the fixture by means of a hub integral with the blisk which is tightened with seven screws using a counter torque wrench in order to save the cyclic symmetry of the structure as much as possible. The rig was designed to hold 30kg (294N) for each damper which is a realistic centrifugal force on a real UPD having a mass of about 5g.

3.1 The dummy disk

The dummy disk was manufactured in order to fulfil two requirements: i) to test the electromagnetic excitation system and the control software of the rotating force and ii) to study the dynamic behaviour of a cyclic structure with underplatform dampers (UPDs) under a specific engine order *EO* excitation in order to validate the numerical model of the blisk with friction contacts between blade platforms and UPDs. The FE model of the blisk is shown in Figure 10 a). The mode shapes of a bladed disk are characterized by a number of *Nodal Diameter* (*ND*), i.e., lines passing for the center of the bladed disk where the modal displacement is null. As an example, Figures 10 b)-d) show modes at ND=0,2,4. In particular, only one mode is associated to ND=0 (the so called umbrella mode) and to ND=N_b/2 while two modes share the same *ND* when 0<*ND*<N_b/2. In this case the natural frequencies of the two modes are equal and the two modes are orthogonal (their scalar product is null). This information can be resumed in a plot where the natural frequencies are plotted with respect to *ND* (Figure 11). Lines connecting the natural frequencies define the modal families of the blisk where modes share a type of motion of the sector. In this case, for instance, the first family (lower frequencies) is characterized by the first bending mode (1F) of the blade, while the second family (higher frequencies) is characterized by the second bending mode (2F, edgewise) of the blade. Label 'free' refers to the modal analysis of the blisk without damper while 'stick' refers to the modal analysis of the blisk coupled to the cylindrical underplatform damper. The 'stick' condition is simulated by constraining the UPDs to the blade platforms through hinge constraints along the line contacts between the cylindrical surface of the UPD and the flat surface of each platform. A cylindrical cross section of the damper is chosen (Figure 11 b)) in order to guarantee the contact between UPDs and blade platforms the simplest as possible. The design aimed at obtaining the first bending mode well isolate from the second bending mode in order to obtain a simple kinematics of the blade platforms in contact with the UPDs. Moreover, a 45° stagger angle is chosen for the blades since both 1F and 2F modal families must have components along the out-of-plane direction since the motion is detected by a Laser Doppler Vibrometer (LDV) which measures the orthogonal component of the velocity with respect to the plane of the blisk.

(a)

(b) ND=0
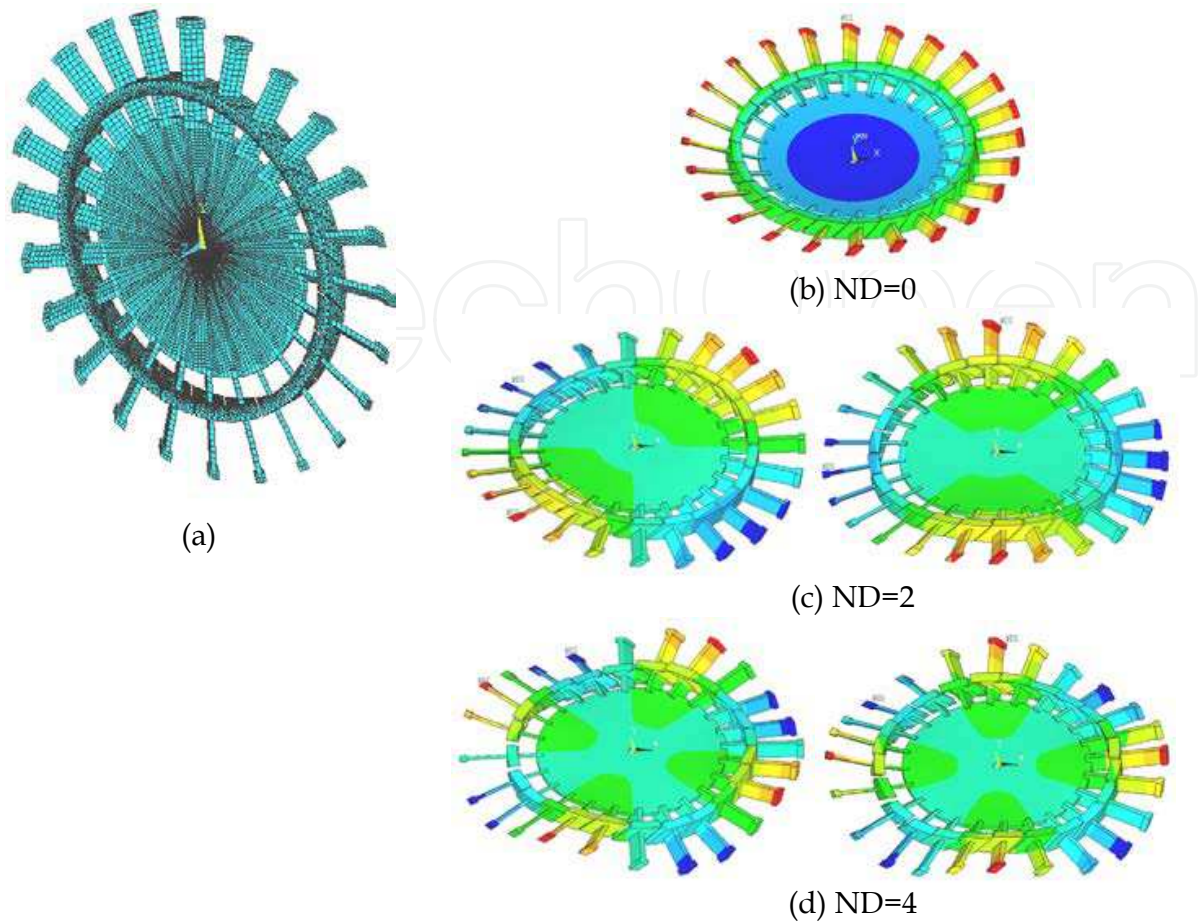
(c) ND=2

(d) ND=4

Fig. 10. a) FE model of the blisk; b) umbrella mode (*ND*=0); c) *ND*=2 orthogonal modes; d) *ND*=4 orthogonal modes.

(a)   (b)
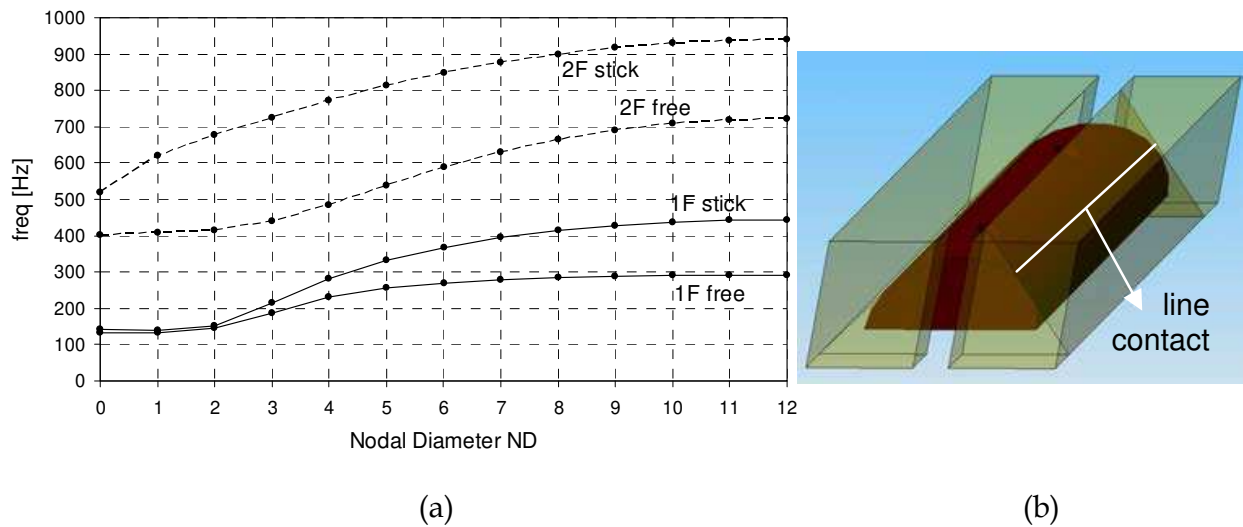
Fig. 11. a) First two bending families, without UPDs (free condition) and with UPDs constrained between the platforms (stick condition); b) line contacts between UPD and platforms.

It can be also noticed that in fully stick condition the highest frequency of the 1F family is under the threshold of 500 Hz. This requirement is determined by the EM currently used; it

is possible to see from Figure 5, in fact, that the value of admittance drops for values of electrical frequency higher than f_{el}=200Hz (i.e. 400Hz mechanical frequency). This means that a too high voltages V may be required to excite the blisk for frequencies higher than f_m=400Hz if the required force amplitude F_A is of the order of magnitude of 10N. For this reason the study will be restricted to the first modal family (1F).

4. The excitation system under the disk

In the final configuration, each EM is positioned under the corresponding blade with an air gap of 2mm. However, before placing all the EMs, different tests are performed by mounting only the FMEM under the disk on a housing purposely machined in the aluminum base (Figure 12). In this case the FMEM is facing the blade instead of the ferromagnetic anchor of the calibration bench.
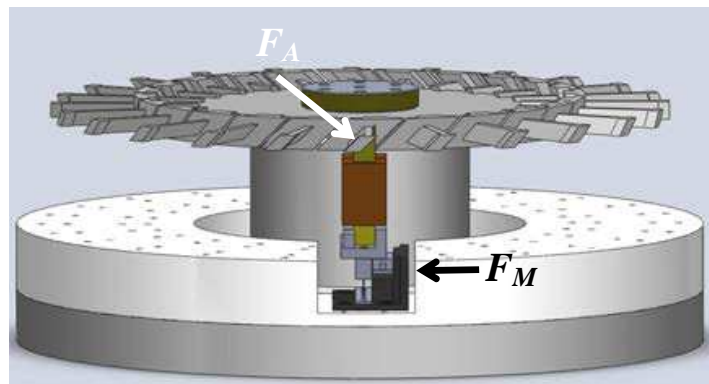
Fig. 12. The FMEM mounted under the disk.

Different tests are performed with the software control in order to obtain the desired $F_{A,nom}$ on the blade. The control is performed by the measurement of F_M (Figure 12). The software adjusts the voltage value until the desired value of force amplitude $F_M = (F_M/F_A)_{AVG} \cdot F_{A,nom}$ is reached by the transducer. This force control is repeated for different $F_{A,nom}$ and for different frequencies f_{el}. In each case the feeding input voltage amplitude V is recorded. In Figure 13 the voltage amplitude V is plotted versus the input electrical frequency f_{el} for different $F_{A,nom}$ values.
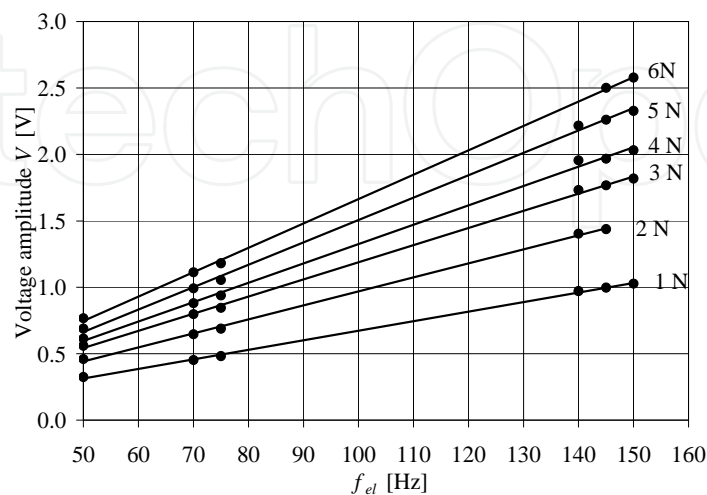
Fig. 13. Feeding voltage amplitude V vs. electrical frequency f_{el} for different excitation force amplitude $F_{A, nom}$.

It can be seen that the trend V vs. f_{el} is still linear for a given value of the force amplitude exciting the blade (compare with Figure 6 b) where the same measurement was performed on the calibration bench at F_A=5N). These tests confirm again the first theoretical relationship of Eq.(10). Moreover, the plots V vs. $\sqrt{F_{Anom}}$ (see Figure 14) are also linear for different electrical frequency values f_{el} confirming the second theoretical relationship of Eq.(10).
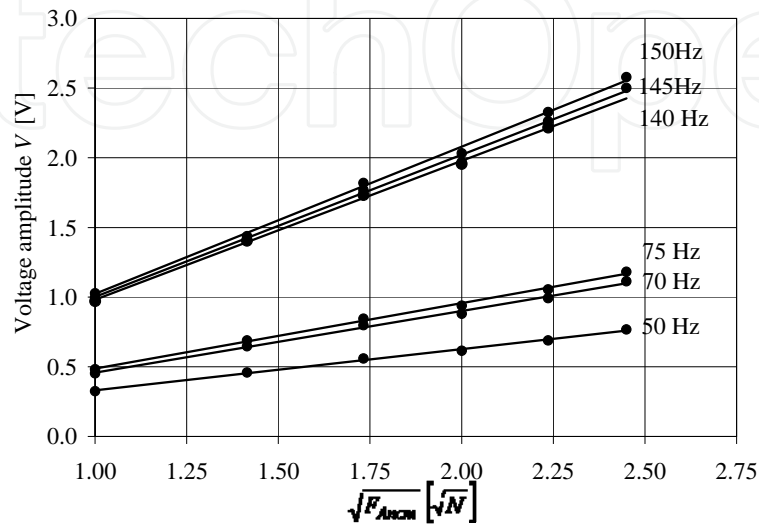

Fig. 14. Feeding voltage amplitude V vs. the square root of the excitation force amplitude F_A for different electrical frequencies f_{el}.

The linear trends V vs. f_{el} and V vs. $\sqrt{F_{Anom}}$ allow to calculate by interpolation the needed input voltage also for force amplitudes or for frequency values different from those employed during the calibration of the FMEM. It is interesting to compare the trends V vs. f_{el} obtained on the calibration bench (dashed lines) and under the disk (solid curves) for two different values of $F_{A,nom}$ (1 N and 5 N) as shown in Figure 15.
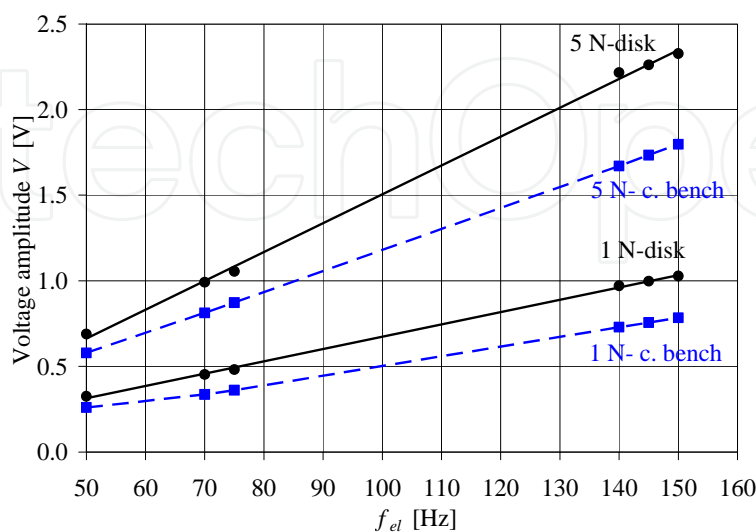
Fig. 15. Comparison of the feeding voltage amplitude V vs. electrical frequency f_{el} when the FMEM is on the calibration bench (dashed line) and under the blisk (solid lines).

It can be noted that higher input voltages are requested by the EM under the disk with respect to the case of the calibration bench in order to obtain the same value of $F_{A,nom}$. The difference is higher for higher frequencies. The difference of the input voltages is due probably to the higher magnetic field loss in the blade connected to the disk compared to the case of the single magnetic anchor on the calibration bench. This voltage difference between the blisk and the calibration bench highlights the importance of having a device like the FMEM which measures the force directly under the disk. The bench calibration of each EM is not enough since the calibration curve does not correspond to the desired $F_{A,nom}$ under the disk.

4.1 Verification of the blisk linearity

The main objective of the tests performed on the dummy blisk is the measurement of the amount of nonlinear friction damping introduced by the UPD. For this reason it must be verified that another source of nonlinear damping is not introduced by the test rig itself and in particular by the contact interface between the blisk and the central hub. The verification of the blisk linearity requires the measurement of the vibration response of the blades. The measurement is performed by means of the scanning LDV which detects the blade velocity along the disk axial direction. One measurement point is chosen for each blade in the same position.

The FMEM is positioned under the bladed disk (as shown in Figure 12) and a harmonic force is applied at different amplitude F_A gradually increasing in order to verify that the blade response measured by the LDV increases proportionally.

The FMEM is fed with an alternate voltage at an electrical frequency f_{el}, the mechanical excitation frequency value f_m (that is two times f_{el}) is chosen as far as possible from both the disk and FMEM natural frequencies in order to avoid calibration complications due to disk or FMEM dynamics. The disk and the FMEM Frequency Response Functions (FRF) measured by impact testing are shown in Figure 16.
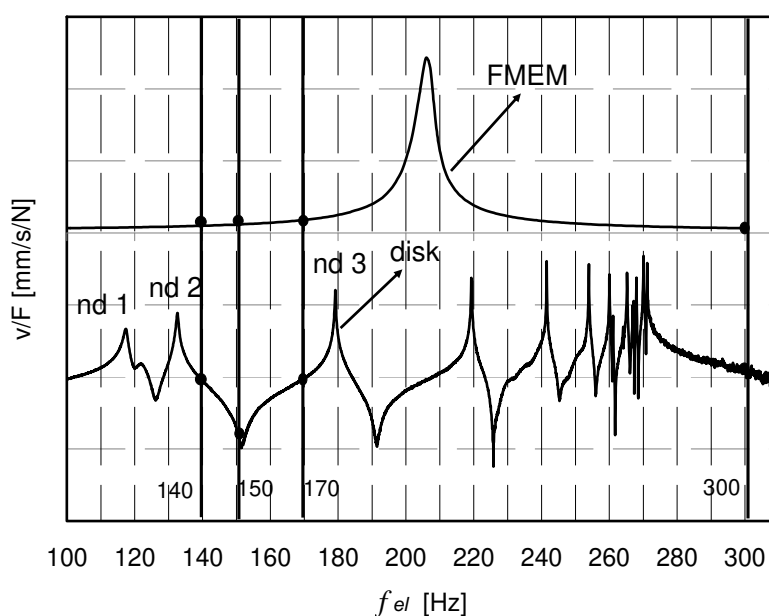

Fig. 16. FRF for the FMEM and for the bladed disk (y-axis is not to scale).

The verification of the disk linearity is performed at two different mechanical excitation frequencies (f_m=150Hz and 300Hz that is, f_{el}=75Hz and 150Hz) which are far from both the disk and FMEM natural frequencies. Once the force control loop has reached the target value F_A at f_m=2f_{el}, a trigger signal activates the scanning LDV to measure the velocity amplitude of the 24 blades. The blade velocity amplitudes vs. the blade number (*velocity profile*) can then be plotted.

In Figure 17 and Figure 18 the "velocity profiles" obtained for different excitation force $F_{A,nom}$ amplitude values are plotted in the case of f_{el}=75Hz and in the case of f_{el}=150Hz. It is possible to see that the velocity profile (see red dots for clarity) increases linearly with the force amplitude F_A. The comparison of the ratios of the different force amplitudes applied to the bladed disk and the corresponding average ratios of the velocity values marked with red
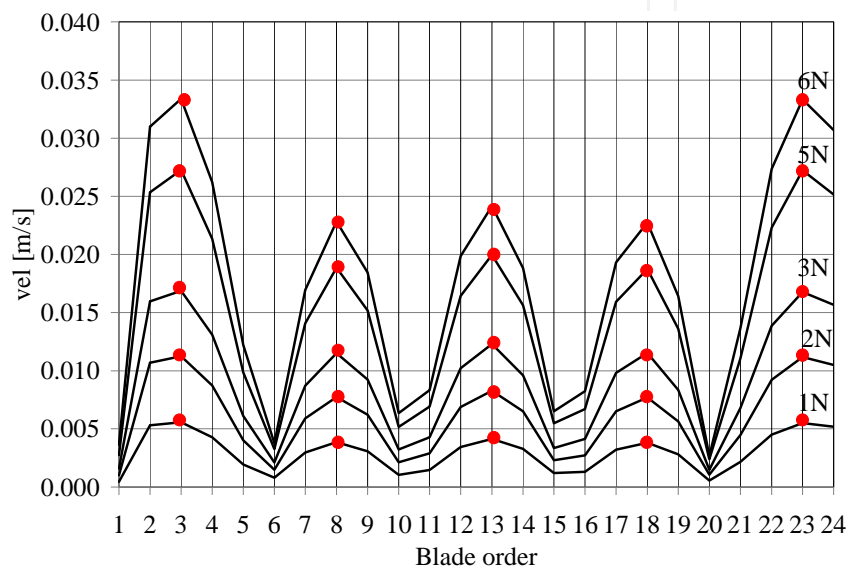
Fig. 17. Blade absolute velocity values for different excitation force amplitude, electrical frequency f_{el}=75 Hz.
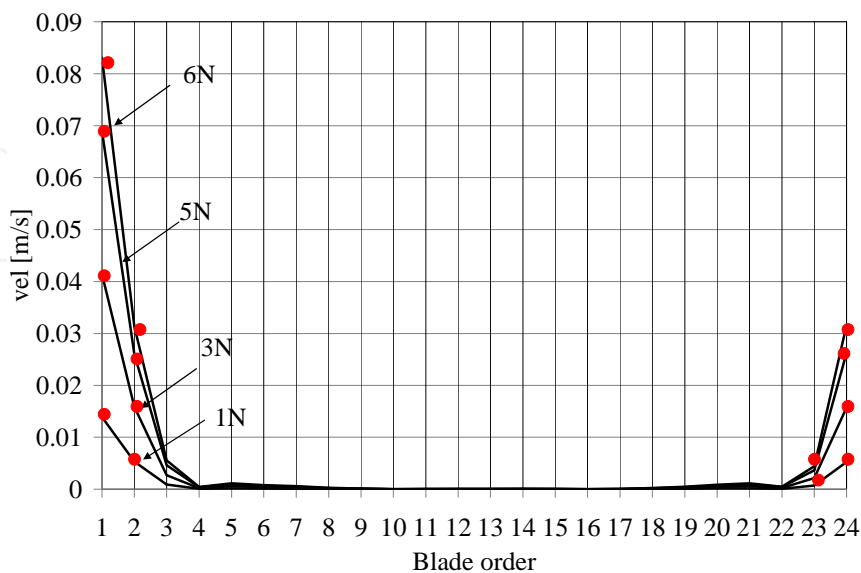
Fig. 18. Blade absolute velocity values for different excitation force amplitude, electrical frequency f_{el}=150 Hz.

dots shows a difference within 2% in the most cases, i.e., within the force value repeatability allowed by the FMEM. As a consequence, the dynamic response of the bladed disk without UPDs can then be considered linear.

4.2 The method for tuning the EMs

In order to obtain the same amplitude of the excitation force for each EMs a tuning process of the magnetic forces is necessary in order to adjust the input voltage for each exciter. The tuning involves an iterative process exciting directly one blade each time and measuring the indirectly excited blade responses. Two system configurations are needed for this calibration:

- configuration 1: only the FMEM is needed under blade 1;
- configuration 2: the 24 EM units are positioned under the bladed disk (after removal of the FMEM).

In the configuration 1 the FMEM is fed with an alternate voltage at the electrical frequency f_{el}. The control software adjusts the voltage amplitude in order to reach the target force value $F_{A,nom}$. As in the case of the blisk linearity verification the scanning LDV measures the velocity amplitude of the 24 blades as a "reference velocity profile" (blade velocity amplitudes vs. the blade number) which is recorded together with the voltage amplitude V and the electrical frequency f_{el}. The mechanical excitation frequencies f_m chosen for the tuning process (140, 150, 170, 300Hz) are highlighted in Figure 16. The chosen mechanical excitation frequency values are far from the disk and from the FMEM natural frequencies. In order to excite the blisk with these excitation frequencies in configuration 1 the FMEM must be supplied with an input voltage with half the value of the electrical frequency (f_{el} = 70, 75, 85, 150Hz). The velocity profiles are plotted in Figure 19 and Figure 20 for the four values of f_{el} feeding the FMEM.
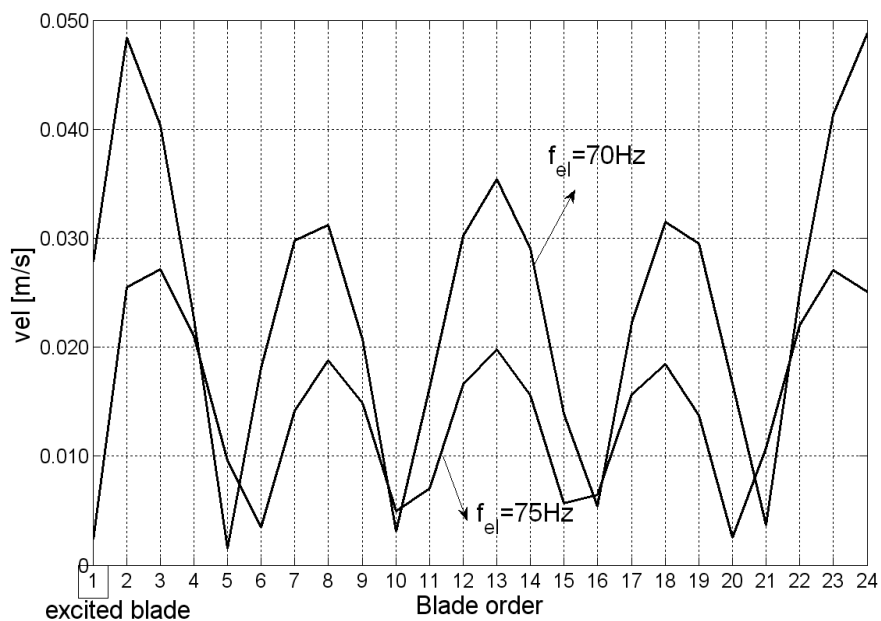

Fig. 19. Velocity amplitude profiles when the FMEM is switched on, force controlled to a nominal force amplitude $F_{A,nom}$=5N, electrical frequency 70Hz and 75Hz.
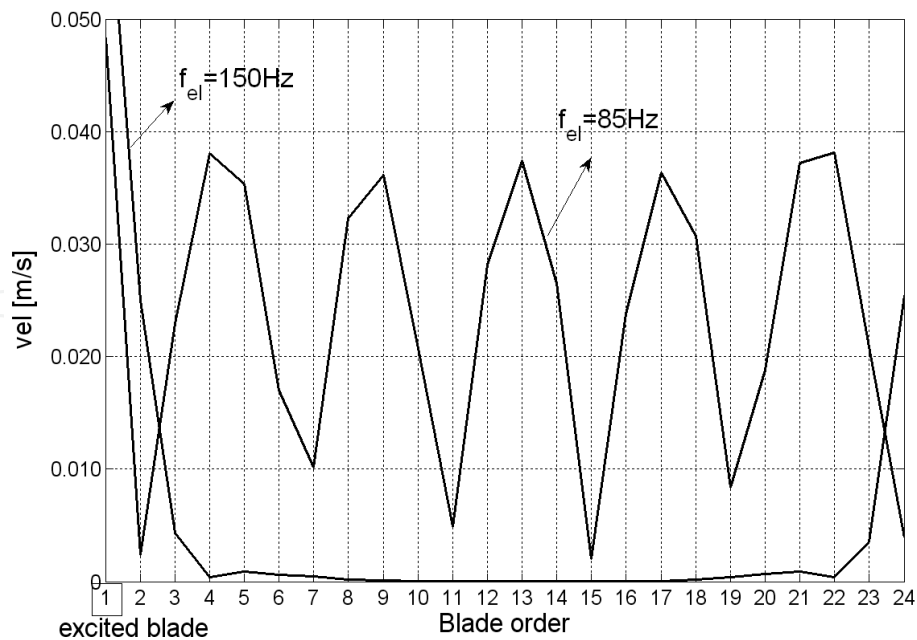
Fig. 20. Velocity amplitude profiles when the FMEM is switched on, force controlled to a nominal force amplitude $F_{A,nom}$=5N, electrical frequency 85Hz and 150Hz.

The velocity profiles of Figure 19 and Figure 20 are kept as reference profiles for the tuning process since they are obtained with a known force amplitude of 5N (measured on site) on the excited blade. Repeatability tests performed after repositioning the FMEM under the disk proved that the repeatability error of the profiles of figure 19 and 20 is lower than 3%.

The system is then set up according to the configuration 2: the FMEM is removed and the 24 EMs are positioned under the blisk. Only one EM per time is switched on. Figure 21 shows the 24 velocity amplitude profiles at the excitation electrical frequency f_{el}=75Hz when the calibration curves of Figure 6 b) are used to set the initial voltage amplitude V for the 24 EMs.
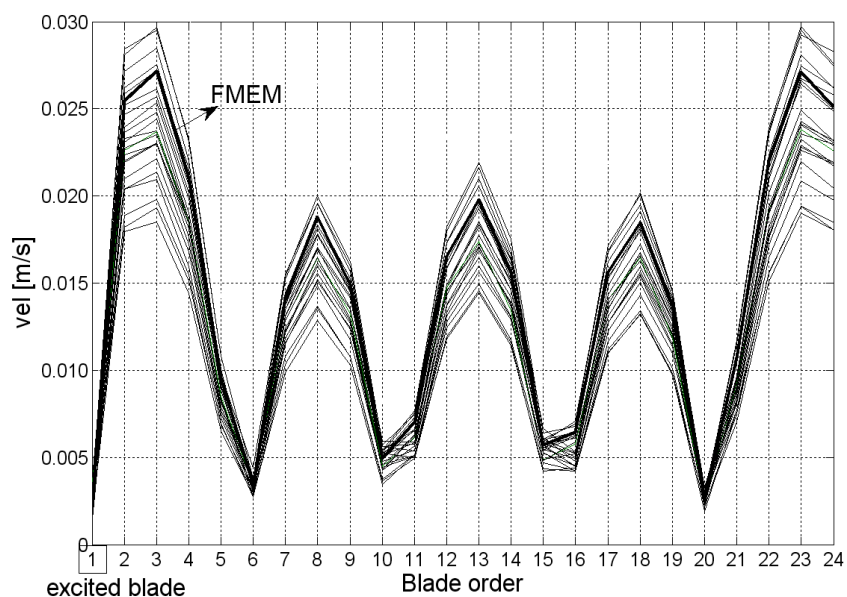
Fig. 21. The 24 velocity profiles, each of them measured with one EM switched on, at f_{el}=75Hz and nominal force amplitude $F_{A,nom}$ =5N, before tuning.

Each velocity profile is measured when only one EM per time excites the structure. The velocity amplitude of the directly excited blade is plotted always in the first position (*Blade Order 1*). On the same figure the velocity reference profile (bold line) obtained with the FMEM at f_{el}=75Hz in the previous step (configuration 1) is plotted. The curves of Figure 21 point out two phenomena:

- there are relevant differences among the velocity profiles when the working EM exciter changes (the standard deviation of the force values compared to the mean value of the force is about 16%),
- the velocity profile obtained by FMEM is inside the profile dispersion of the other 24 EMs.

Considering the dynamics of the blisk linear as proved before and neglecting the presence of mistuning phenomena since the excitation frequency is far from resonance conditions, the differences among the profiles in Figure 22 must be referred to different excitation force amplitudes. These differences are not related to the manufacture of the EM units since they are taken into account in the calibration curves of Figure 6b). Other causes producing different velocity profiles are probably due to i) different positions of the EMs under the disk blades that cause different air gaps, ii) different shape and material properties of the blade compared to the anchor used for calibration. These differences among the EMs highlight the importance of having a FMEM measuring the real force amplitude on site (i.e. under the disk). The 24 EMs can than be tuned to the reference FMEM. The tuning process aims at adjusting the voltage on the 24 EMs until they produce the same velocity profiles of the blisk as the one measured with the FMEM. A method is here proposed starting from the velocity profiles shown in Figure 21. The voltages are adjusted in order to obtain 24 velocity profiles overlapping the FMEM reference profile as shown in Figure 22.
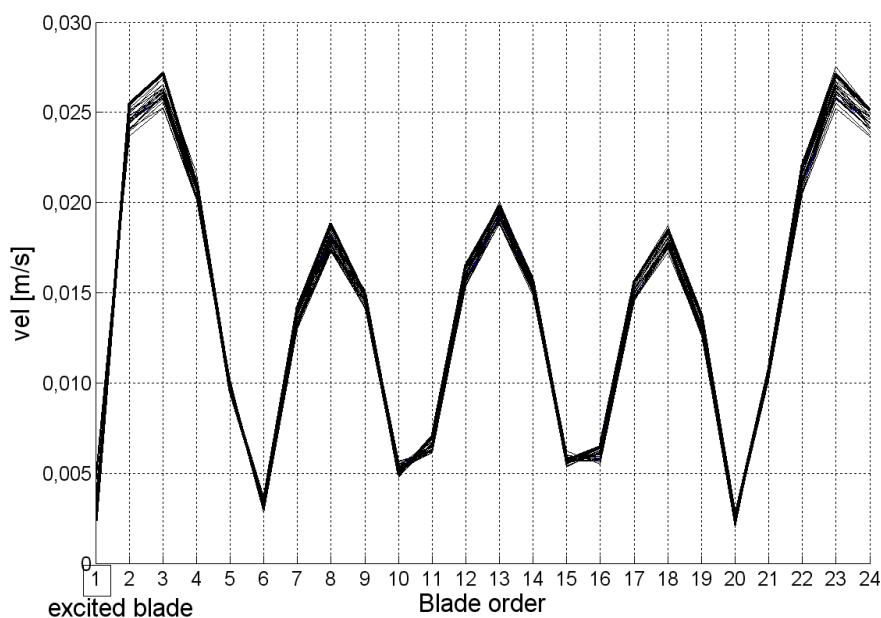

Fig. 22. The 24 velocity profiles, each of them measured with one EM switched on, at f_{el}=75Hz and nominal force amplitude $F_{A,nom}$=5N, after tuning.

In detail the method works as follows. Let $\dot{X}_{be}$ and $\dot{X}_{bFMEM}$ be the measured velocity amplitudes of the blade corresponding to the blade order b when respectively the EM e and

the FMEM is switched on. Considering the system linear and assuming the FMEM as a reference, the ratio $\dot{X}_{be} / \dot{X}_{bFMEM}$ is proportional to the excitation force ratio $F_{A,e} / F_{A,FMEM}$ where $F_{A,e}$ is the actual excitation force amplitude on the blade facing the EM e and $F_{A,FMEM}$ is the nominal value of the force (in this case 5N).

For each response of Figure 21 (corresponding to the e-th EM working) the correction factor k_e is calculated as:

$$k_e = mean\left(\frac{\dot{X}_{be}}{\dot{X}_{bFMEM}}\right), \quad b = 1,...,N_b \tag{11}$$

In order to get the same force amplitude for each EM unit the force is corrected as $F_{A,e}^* = F_{A,e}/k_e$ by adjusting the input voltage as $V_e^* = V_e / \sqrt{k_e}$ since the voltage is proportional to the square root of the force (Eq.10). The velocity profiles plotted in Figure 22 are measured after two iterations of the tuning process at f_{el}=75Hz. The dispersion of the force amplitude corresponding to the different velocity profiles with respect to the nominal value of 5N are less than 2%. It can be concluded that after this tuning process each of the 24 EMs produces on the excited blade the same force amplitude of 5N with a dispersion of 2%. The same calibration procedure is repeated for the other electrical frequency values (f_{el} =70, 85, 150Hz) in order to characterize the linear trend of the voltage as a function of frequency when the same force $F_M = (F_M/F_A)_{AVG} \cdot F_{A,nom}$ is required, as it was done in the calibration bench (Figure 13) with the FMEM. The voltage values at frequencies not directly tuned can be found by linear interpolation since the experimental evidence verifies the linear trends of Eq.(10).

It must be noted that the tuning method here proposed is very efficient since it avoids the calibration of one EM at a time on a separate bench which is time consuming. In fact, the tuning process does not require a particular starting voltage values of the EMs, in particular it is not necessary to start with voltage values coming from the EMs calibration (Figure 6b).

5. Example of test results

The test campaign is performed for the modes at ND=2, 4 without dampers (free, linear configuration) and with UPDs (nonlinear configuration). Each mode is excited with a travelling wave with an engine order EO=ND. First, two forced responses at two different excitation frequencies are shown for the blisk without damper (free system), second the FRFs are shown in terms of mobility, for the two ND at 7 different values of force amplitude F_{Anom} =0.1, 0.2, 0.3, 0.6, 1, 2.5, 5N when UPDs are mounted. Each FRF is the envelope of the maximum value of the FRF of the 24 blades at each frequency. The test results are selected since they show the capability of the rig to detect both the effect of the friction damping on the blisk dynamics and the presence of mistuning.

5.1 Forced response of the blisk without UPDs under the travelling force

A rotating force is generated in order to excite the ND=2 rotating mode shape. For this reason the voltage signal is generated for each EM in order to obtain a force pattern on the EMs equal to:

$$f_{a,n} = F_{Anom} \cos\left(f_m \cdot 2\pi t + (n-1)\frac{2\pi}{N_b}EO\right) \tag{12}$$

$$n = 1,....,N_b \qquad f_m = 2f_{el}$$

where *EO* is chosen equal to 2 in order to excite the ND=2 rotating mode shape. The force amplitude F_{Anom} is in this case very low since the system is linear (F_{Anom}=0.2N). The response is measured by measuring one point per blade by means of the scanning LDV in order to measure the rotating mode shape along the hoop direction of the blisk. The voltage signal of the first EM is used as a trigger in order to sinchronize the 24 signals measured by the LDV in 24 different time instants. The blisk is excited at f_m=134Hz which is far from the natural frequency f_{1F}=131Hz of the ND=2 rotating mode shape, first family. Figures 23 a)-d) show the
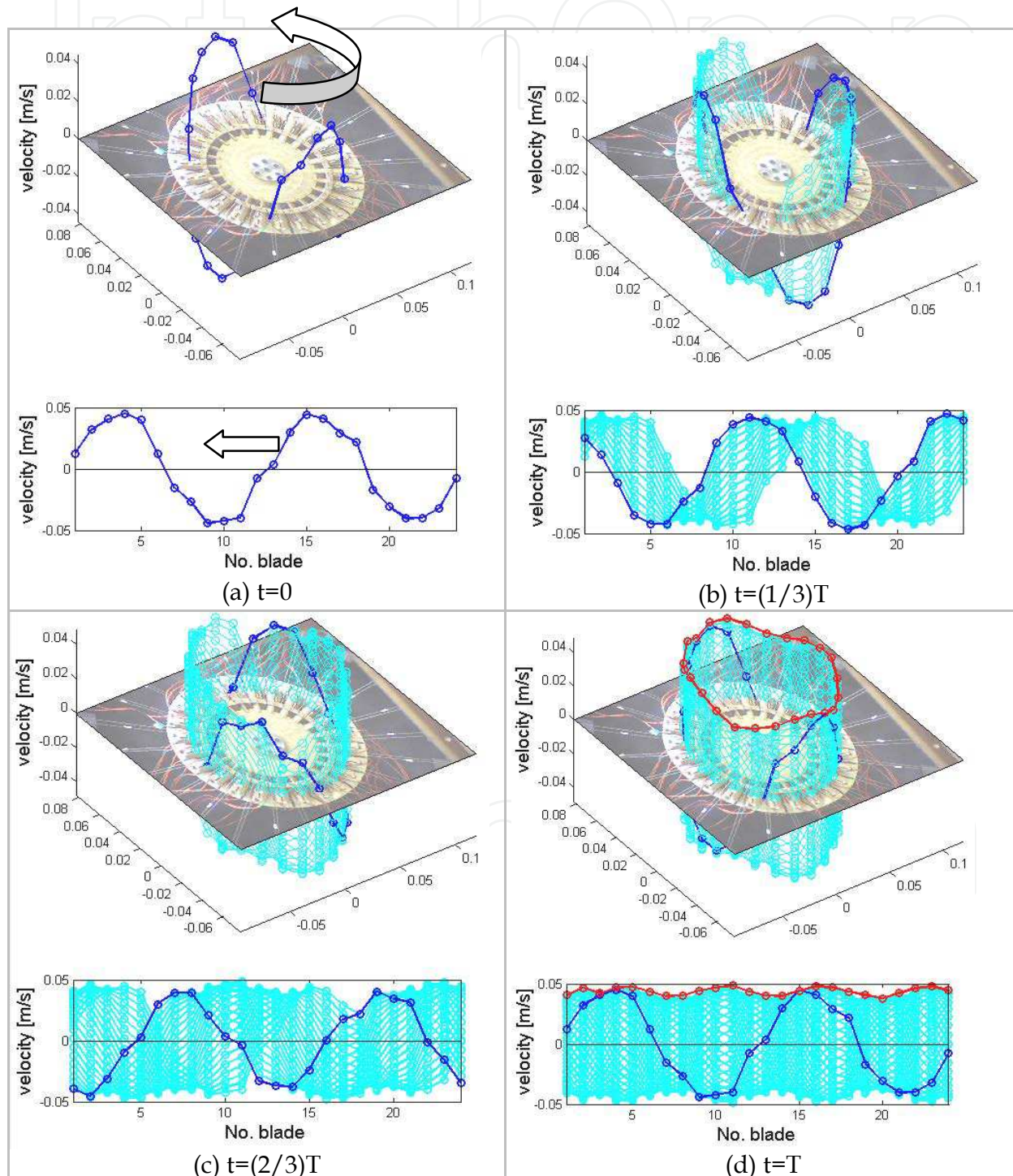
Fig. 23. Rotating Deformed Operative Shape, ND=2, EO=2, far from resonance.

Operative Deformed Shape (ODS) of the blisk for four equally spaced time istants within a complete rotation of the travelling force $T=EO(1/f_m)$. It is possible to see how the two orthogonal mode shapes as seen in the simulation of Figure 10 c) combines to generate a rotating mode shape at ND=2 following the rotating force. Figure 23 d) shows all the steps after one rotation is complete, the red line groups the maximum amplitude that each blade reaches in order to prove that the difference in amplitude is acceptable. If the same test is performed at a frequency which is closer to the natural frequency of the 1F mode, ND=2 (Figure 24 a)-d)), it is possible to see that the blades vibrate with different amplitudes proving the existence of inherent mistuning due to the asymmetries produced by the manufacture or the constraint. However, the mistuning can be considered 'small' since it only perturbs the ND=2 shape of the rotating mode which can be still identified and does not localize the energy of the system to a small number of blades.


(a) t=0

(b) t=(1/3)T

(c) t=(2/3)T

(d)t=T
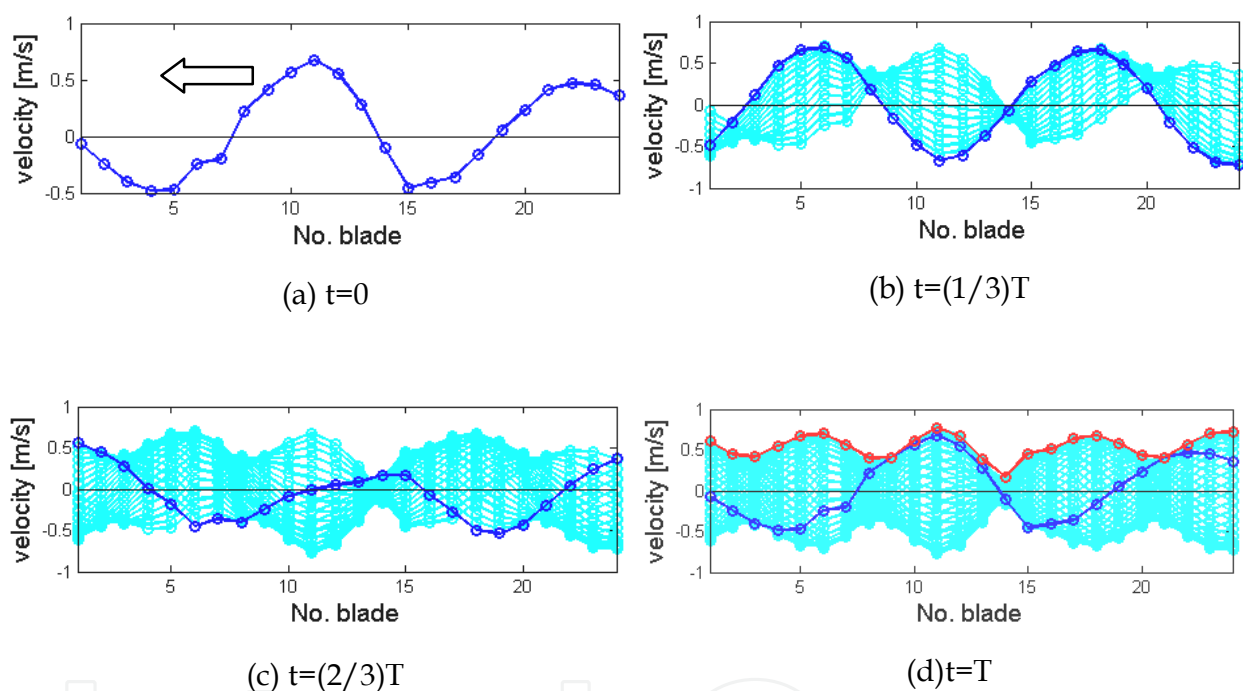
Fig. 24. Rotating Deformed Operative Shape, ND=2, EO=2, resonance condition.

5.2 The forced response with friction damping

The UPDs are positioned in their cavities and each of them is loaded with an equivalent centrifugal load of about 50N (5kg of dead weights) (Firrone et al., 2011). In Figure 25 the free (linear) and the nonlinear FRFs at ND=2 are plotted as the envelope of the maximum value of the FRF of each single blades at each frequency. The FRFs show that the amount of damping depends on the force amplitude value F_{Anom}. When F_{Anom} is low (F_{Anom}=0.1N) the relative displacement at the contacts is not large enough to provide a large amount of damping. At the same time the UPDs act more as an additional constraint whose main effect is to stiffen the structure as demonstrated by the increase of the frequency value of the peaks with respect to the free response. As the excitation force amplitude increases (F_{Anom}=0.2N, 0.3N), more
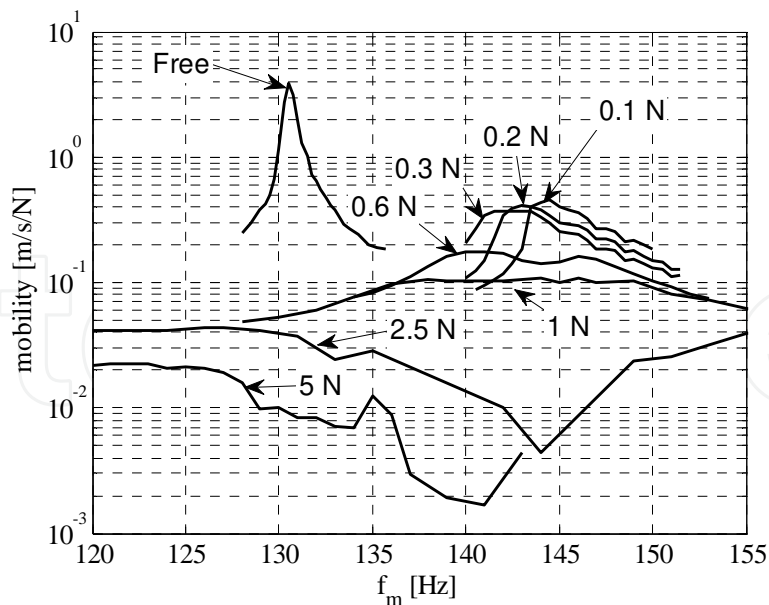
Fig. 25. FRF of the bladed disk (free and with UPDs) for different amplitude values F_A of the excitation force. CF =50N, $EO=ND$=2.

damping is provided to the bladed disk, a general reduction of the vibration amplitudes of the blades is observed and the distance of the peak frequency from the corresponding '*free*' value decreases since large relative displacements at the contacts globally determine a less stiff constraint for the blades. As the excitation becomes larger and larger (F_A=1N, 2.5N, 5N) the smooth peak is almost flattened while the frequency peak tends toward values lower than that of the free response since the UPDs act as an additional mass of the blisk. These results can be summed up as shown in Figure 26 in terms of the optimization curve where the frequency and the amplitude values of the response peaks are plotted vs. the variable parameter CF/F_{Anom}. It is possible to see that a minimum response of the blisk amplitude mobility exists corresponding to an optimum combination of damper mass (i.e., CF) and amount of excitation (i.e., F_{Anom}).
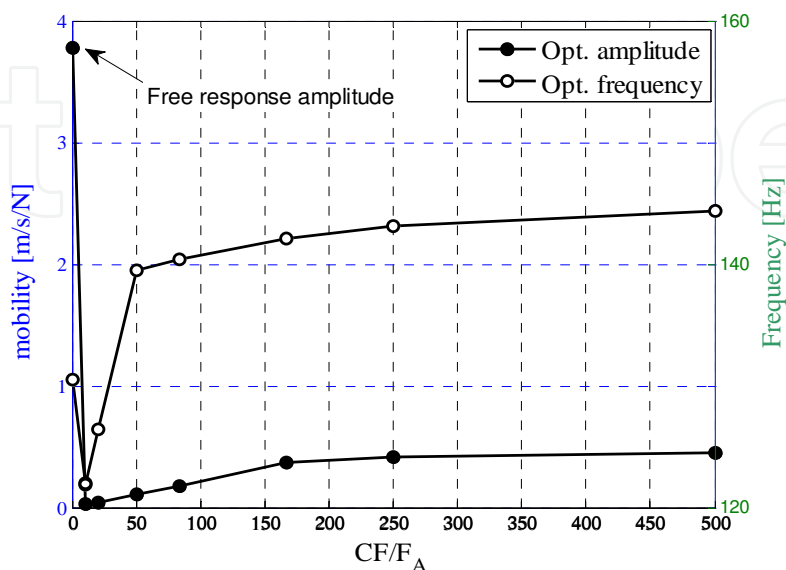

Fig. 26. Optimization curves at ND=2.

5.3 The forced response with mistuning introduced by the friction dampers

In order to show the effect of mistuning introduced by the UPD, the rotating mode shape ND=4 is excited with a travelling force at EO=4. In Figure 27 two peaks are clearly visible for low values of F_{Anom} (F_{Anom}= 0.1, 0.2, 0.3N) for f_m=316Hz and 345Hz. The presence of two peaks instead of one is an index of presence of mistuning since the lack of cyclic symmetry causes the split of the natural frequency of the 'twin' modes at ND=4. This can be verified by plotting the Operative Deformed Shape (ODS) of each blade when the maximum absolute value of the velocity during the blisk vibration is reached. The two stationary mode shapes vibrate at resonant conditions for two different frequency values and the rotating response of the blisk is no more obtained.
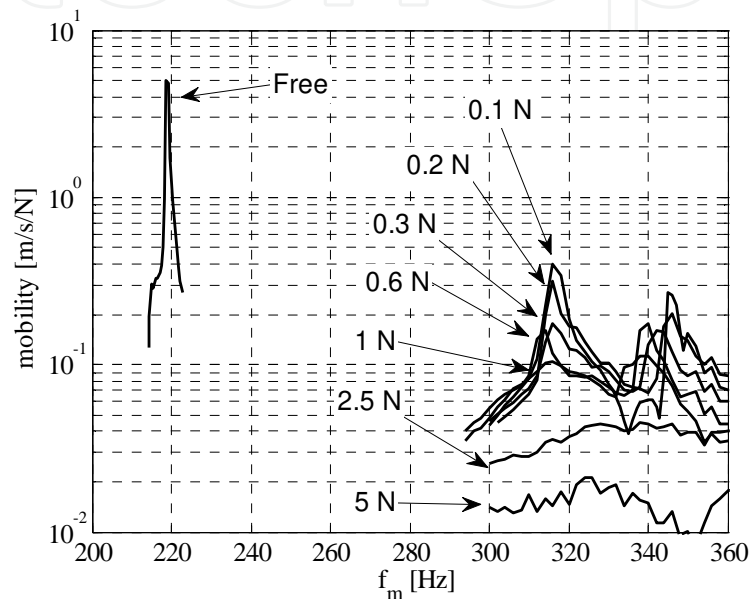

Fig. 27. FRF of the bladed disk (free and with UPDs) for different excitation force amplitude values. CF =50N. EO=4.
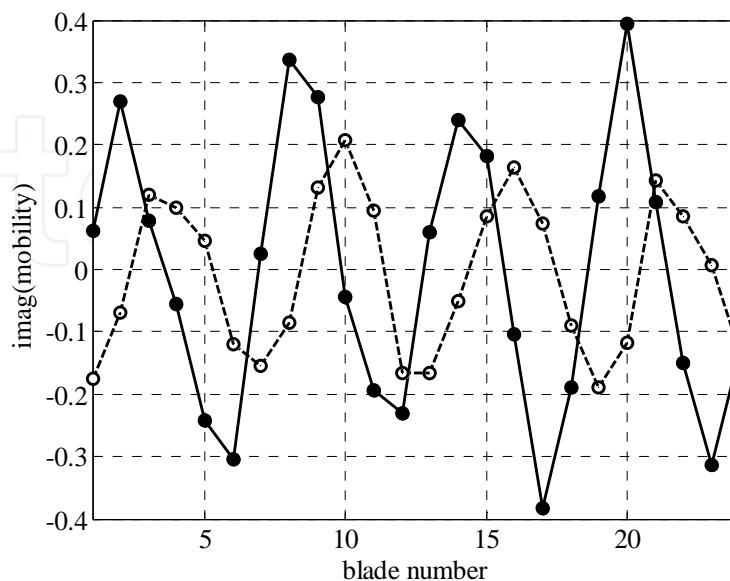

Fig. 28. Maximum amplitude of the ODS (mobility) for the different blades at 316Hz (solid line) and 345Hz (dotted line), F_{Anom} =0.1N, EO=4.

In particular, the ODS for the two peak frequencies are plotted for the case F_{Anom}= 0.1N in Figure 28. It can be noted that each maximum amplitude of the ODS represents a mode shape ND=4 (4 maxima are present). Moreover the two mode shapes of Figure 28 are orthogonal. This consideration puts in evidence that the two peaks of Figure 27 are the mistuned 'twin' modes at ND=4.

Figure 27 suggests another important consideration. By increasing F_{Anom} more damping is provided in the system and the two mistuned peaks become flat and disappear confirming that the right amount of damping can mitigate the mistuning phenomenon. The test rig proved then to be able to put in evidence the interaction of friction damping and mistuning.

6. Conclusions

The design, calibration procedure and testing of a complete (hardware and software) non-contact excitation system is presented. The system aims at performing accurate measurements of the dynamic behaviour of bladed disks in presence of mistuning and nonlinearity due to friction contacts. The system yields accurate results and it is characterized by three key features.

First, the purposely designed EMs generate force amplitudes that can be considered high for a noncontact excitation system. Each EM can reach a force amplitude up to 10 N (up to 300Hz excitation frequency of the system) and 5 N (up to 600 Hz). The several features affecting this force value are highlighted.

Second, thanks to a novel calibration method performed on site under the disk to iteratively calibrate the force, differences of force amplitudes among the blades are highly reduced (2% variation among force amplitudes). The method is efficient since it avoids the calibration of each EM (one by one) separately which is time consuming and in any case it proved to be inaccurate when the EMs are mounted under the blisk.

Third the value of the force amplitude exciting the blades is known with good accuracy (less than 5% error with respect to the nominal value). This feature is essential for stepped sine, force controlled tests to investigate the nonlinearity due to friction contacts. A device carrying one of the EMs and instrumented with a force transducer is designed, constructed and calibrated for this purpose. The device called FMEM (Force Measurement ElectroMagnet) is able to measure the force directly on site under the disk and is used as a reference for the other EMs during calibration.

The travelling excitation system is applied to the test rig Octopus where an integral bladed disk carries underplatform dampers (UPDs) which introduce nonlinearities due to friction.

The test campaign provided an example of results which proved that the system is capable of an engine order type excitation at different controlled force amplitudes. The developed noncontact travelling excitation system together with a noncontact laser Doppler vibrometer measurement of the response highlight 1) the effectiveness of the UPDs in reducing the blades vibration amplitude at different EOs, 2) the interaction of the damping provided by the UPDs and the introduction of mistuning.

7. Acknowledgment

8. References

Avalos, J. & Mignolet, M. P. (2008) On damping entire bladed disks through dampers on only a few blades, GT-2008-51446, *Proceedings of the of ASME Turbo Expo*, June 9-13, Berlin, Germany.

Beirov, B., Kühhorn, A., Schrape, S. (2008). A discrete model to consider the influence of the air flow on blade vibrations of an intergral blisk compressor rotor, *Proceedings of the of ASME Turbo Expo*, June 9-13, Berlin, Germany.

Beirov, B., Kuhhorn, A., Nipkau, J. (2009). On the influence of strain gauge instrumentation on blade vibrations of integral blisk compressor rotors applying a discrete model, GT2009-59207, *Proceedings of the of ASME Turbo*, June 8-12, Orlando, Florida.

Berruti, T. (2010). A test rig for the investigation of the dynamic response of a bladed disk with underplatform dampers, *Mechanics Research Communications*, vol 37, doi:10.1016/j.mechrescom.2010.07.008, pp 581-583.

Berruti, T., Firrone, C.M., Gola, M.M. (2010). A test rig for non-contact travelling wave excitation of a bladed disk with underplatform dampers, GT2010-22879, *Proceedings of the of ASME Turbo*, Glasgow, UK., pp.1-9.

Berruti, T., Firrone, C.M., Gola, M.M. (2011). A test rig for non-contact travelling wave excitation of a bladed disk with underplatform dampers. *Journal of Engineering for Gas Turbines and Power*, Vol 133, pp. 032502-1-8, ISSN 0742-4795, DOI: 10.1115/1.4002100.

Castanier, M. P. & Pierre, C. (2006). Modeling and analysis of mistuned bladed disk vibration : Status and emerging directions. *Journal of Propulsion and Power*, Vol. 22, Issue 2, pp.384-396, DOI: 10.2514/1.16345. ISSN 0748-4658.

Firrone, C.M., Berruti, T. (2011). An electromagnetic system for the non-contact excitation of bladed disks, *Experimental Mechanics*, DOI: 10.1007/s11340-011-9504-1.

Firrone, C.M, Berruti, T., Gola, M.M. (2011). On force control of an engine order type excitation applied to a bladed disk with underplatform dampers, IDETC2011-47255, *Proceedings of the International Design Engineering Technical Conferences (IDETC)*, Washington, pp. 1-10.

Chang, J. Y. & Wickert, J. A. (2002). Measurement and analysis of modulated doublet mode response in mock bladed disks", *Journal of Sound and Vibration*, Vol.250, Issue 3, pp-379-400, doi:10.1006/jsvi.2001.3942.

Gilbert, C., Kharyton, V., Thouverez, F., Jean, P. (2010). On forced response of a rotating integrally bladed disk: predictions and experiments, GT2010-23610, *Proceedings of the of ASME Turbo Expo*, June 14-18, Glasgow, UK.

Gotting, F., Sextro, W., Panning, L., Popp, K. (2004). Systematic mistuning of bladed disk assemblies with friction contacts, GT2004-53310, *Proceedings of the of ASME Turbo Expo*, June 14-17, Vienna, Austria.

Heath, S. & Imregun, M. (1998). A survey of Blade Tip-Timing Measurement Techniques for turbomachinery Vibration", *Journal of Engineering for Gas Turbines and Power*, Vol.120, Issue 4, pp.784-791, doi:10.1115/1.2818468.

Heinz, C., Schatz, M., Casey, M. V., Stuer, H. (2010). Experimental and analytical investigations of a low pressure model turbine during forced response excitation, GT2010-22146, *Proceedings of the of ASME Turbo*, June 14-18, Glasgow, UK.

Jones, K.W. & Cross, C.J. (2003). Travelling Wave Excitation System for Bladed Disks", *Journal of Propulsion and Power*, Vol. 19, pp.135-141, ISSN 0748-4658.

Judge, J., Ceccio, S. L., Pierre, C. (2003). Traveling-wave excitation and optical measurement techniques for non-contact investigation of bladed disk dynamics, *The Shock and vibration digest*, Vol. 35, Issue 3, pp.183-910, ISSN 1741-3184.

Kenyon, J.A. & Griffin, J.H. (2003). Experimental Demonstration of Maximum Mistuned Bladed Disk Forced Response. *Journal of Turbomachinery*, Vol. 125, Issue 4, pp. 673-681. doi:10.1115/1.1624847.

Kruse, M. J. & Pierre, C. (1997). An Experimental Investigation of Vibration Localization in Bladed Disks, Part I: Free Response", *Proceedings of the 42nd ASME Gas Turbine & Aeroengine Congress, User's Symposium & Exposition*, Orlando, Florida.

Kruse, M. J. & Pierre, C. (1997). An Experimental Investigation of Vibration Localization in Bladed Disks, Part II: Forced Response", *Proceedings of the 42nd ASME Gas Turbine & Aeroengine Congress, User's Symposium & Exposition*, Orlando, Florida.

Petrov, E., Hennings, H., Di Mare, L., Elliott, R. (2010). Forced response of mistuned bladed discs in gas flow: a comparative study of predictions and full-scale experimental results. *Journal of Engineering for Gas Turbines and Power*, Vol. 132, Issue 5, 052504, doi:10.1115/1.3205031. ISSN: 0742-4795.

Pierre, C., Judge, J., Ceccio, S. L., Castanier, M. P. (2002). Experimental Investigation of the Effects of Random and Intentional Mistuning on the Vibration of Bladed Disks, *Proceedings of the 7th National High Cycle Fatigue Conference*, Palm Beach, Florida.

Prchlik, L., Misek, T., Kubin, Z., Duchek, K.. (2009). The measurement of dynamic vibration modes and frequencies of a large LP bladed disc, GT2009-60002, *Proceedings of the of ASME Turbo Expo*, June 8–12, Orlando, Florida, USA.

Rice, T., Bell, D., Singh, G. (2007). Identification of the stability margin between safe operation and the onset of blade flutter, GT2007-27462, *Proceedings of the of ASME Turbo Expo*, May 14-17, Montreal, Canada.

Sever, I., A. (2004). Experimental validation of turbomachinery blade vibration predictions, *PhD Thesis*, Department of Mechanical Engineering, London.

Strehlau, U. & Kuhhorn, A. (2010). Experimental and numerical investigations of HPC blisks with a focus on travelling waves, GT2010-22463, *Proceedings of the of ASME Turbo*, June 14-18, Glasgow, UK.

Szwedowicz, J., Gilbert, C., Sommer, T. P., Kellerer, R. (2006). Numerical and experimental damping assessment of a thinwalled friction damper in the rotating set-up with high pressure turbine blades", *Proceedings of the of ASME Turbo Expo*, May 8-11, Barcelona, Spain.

Szwedowicz, J., Secall-Wimmel, T., Dünck-Kerst,, P., Sonnenschein, A., Regnery, D., Westfahl, M. (2007). Scaling concept for axial turbine stages with loosely assembled friction bolts: the linear dynamic assessment, part I, GT2007-27502, *Proceedings of the of ASME Turbo Expo*, May 14-17, Montreal, Canada.

Thomas, D. L. (1979). Dynamics of rotationally periodic structures. *International Journal for numerical methods in engineering*, Vol.14, pp. 81-102.
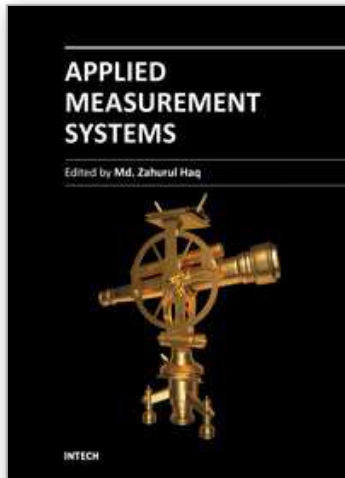
Applied Measurement Systems

Edited by Prof. Zahurul Haq

Measurement is a multidisciplinary experimental science. Measurement systems synergistically blend science, engineering and statistical methods to provide fundamental data for research, design and development, control of processes and operations, and facilitate safe and economic performance of systems. In recent years, measuring techniques have expanded rapidly and gained maturity, through extensive research activities and hardware advancements. With individual chapters authored by eminent professionals in their respective topics, Applied Measurement Systems attempts to provide a comprehensive presentation and in-depth guidance on some of the key applied and advanced topics in measurements for scientists, engineers and educators.

How to reference

In order to correctly reference this scholarly work, feel free to copy and paste the following:

Christian Maria Firrone and Teresa Berruti (2012). Non Contact Measurement System with Electromagnets for Vibration Tests on Bladed Disks, Applied Measurement Systems, Prof. Zahurul Haq (Ed.), ISBN: 978-953-51-0103-1, InTech, Available from: http://www.intechopen.com/books/applied-measurement-systems/non-contact-measurement-system-with-electromagnets-for-vibration-tests-on-bladed-disks

INTECH
open science | open minds